Geoid and Sea Surface Topography from satellite and ground data in the Mediterranean region - A review and new proposals

F. Sansò [(1)], G. Venuti [(1)], I. N. Tziavos [(2)], G. S. Vergos [(2)], V. N. Grigoriadis [(2)]

[(1)] DIIAR - Politecnico di Milano, Polo Regionale di Como - Via Valleggio, 11 - 22100 Como - Italy

[(2)] Department of Geodesy and Surveying, Aristotle University of Thessaloniki, University Box 440, 54124 Thessaloniki - Greece

Accepted *date*. Received *date*; in original form *date*

Abbreviated title: *Geoid and Sea Surface Topography from satellite and ground data. Review and proposals.*

Correspondence to:
George Vergos,
Department of Geodesy and Surveying, Aristotle University of Thessaloniki, Univ. BOX 440, GR-54124, Thessaloniki, Greece,
Tel.: 0030 2310 994225,
Fax: 0030 2310 995948,
email: vergos@topo.auth.gr

ABSTRACT. The determination of local and regional geoid models has been the topic of extensive research in physical geodesy for the last decades. From the initial realizations of astrogeodetic geoid models and combination solutions with few gravity observations, we have sailed through the era of satellite geodesy and the exploitation of altimetric observations which provided an unprecedented view of the geoid and Earth's gravity field over the oceans. From 2000 on, when the gravity field dedicated satellite missions of CHAMP and GRACE have been launched, gravity field and geoid determination have experienced tremendous improvements in the long and medium wavelength of the spectrum, while geoid variations of a few mm attributed to mass variations have been monitored for the first time by space geodetic techniques. The significant improvement in Global Geopotential Model (GGM) determination, with the latest example of EGM08 (Pavlis et *al.*, 2008), and the expected impact of the GOCE mission, which is planned to be launched in 2008, will result in a cumulative geoid error of ±2 cm to degree and order 200.

The drastic improvement in geoid determination through heterogeneous data combination, i.e., gravity anomalies, altimetric sea surface heights, deflections of the vertical, GPS/Leveling geoid heights, potential and its second order derivatives, has also led to the synergy between geodesy and other geosciences. Of special interest is the application of geodetic techniques and products in oceanographic studies and vice versa. In this frame, mean sea surface, sea surface topography and ocean circulation models have been derived from geodetic data and techniques. The key component in all these studies has been the combination of various types of geodetic data, which has been a topic of geodetic research for more than fifty years, originating from the pioneering work of Eeg and Krarup (1975), who first presented the integrated approach of geodetic data adjustment. From that idea stem the origins of the leading estimation principle in modern geodetic research, i.e., that of least squares collocation (LSC), which due to the use of many and various types of data and through the use of Fourier transforms (FT) introduced the use of system theory with geodetic data.

In this context, the present work aims to provide a review of the application of least squares collocation for heterogeneous data combination in studies related to the determination of the geoid and the sea surface topography. First, an outline of the observation equations used in LSC is presented with a derivation of the final geoid height estimates. The application of LSC for mean dynamic topography determination is then presented, together with the implementation of the Multiple Input Multiple Output System Theory for geoid determination. In the same section, a brief outline of the similarities and differences between the two methods is also given. The next section is devoted to the application of LSC in data combination schemes when GOCE observables, i.e., potential and its second order derivatives, are available. It should be noted that within the context of this paper, whenever GOCE observables are mentioned they refer to simulation datasets. Results acquired by the authors towards the determination of geoid models over both land and sea are also presented, while a detailed discussion on the improvement that GOCE data provide is given. The last section is devoted to the presentation of a new method for altimetric sea surface height data analysis and the determination of sea surface topography covariance functions based on second order kriging. Results based on both simulated data and real altimetric sea surface heights are presented using both the traditional LSC approach and second order kriging.

Keywords. Mediterranean geoid, GOCE mission, gravity, altimetry, quasi-stationary sea surface topography.

1 Introduction

This paper summarizes the state of the art of the research conducted by the University of Thessaloniki and Politecnico di Milano in the framework of a Scientific and Technological cooperation agreement supported by the Joint Greek-Italian Committee. The purpose of the project was the study of integrated techniques to determine the geoid and the quasi-stationary sea surface topography for closed sea areas, with a particular focus on the Mediterranean Sea, from satellite and marine data. Satellite data can include satellite altimetry observations of various missions (e.g., ERS1/2, TOPEX/Poseidon, JASON-1, ENVISAT, etc.) and data from the recent and forthcoming satellite missions (e.g., CHAMP, GRACE and GOCE), while ground observations are land, marine and airborne gravity, GPS/Levelling and bathymetry data (Forsberg *et al*. 2007). Re-tracked multi-satellite altimetry sea surface heights close to the coastline (see, e.g., Hwang *et al.* 2006, Kingdon *et al.* 2008, Madsen *et al.* 2007), that in the last years have enriched the available data for gravity, geoid, sea surface topography and ocean circulation modelling, have been included. Since the focus of the paper is not on the combination of global models with local observations, we shall simply assume in the introductory section to Least Squares Collocation that the contribution coming from a global model (e.g., up to degree 180 or 200) is subtracted from everything just to avoid mixing signals with very different orders of magnitude that usually poses numerical problems in data management. Also, after this removal, the ordinary geodetic equations can be used in a spherical approximation form.

So we consider here as observed quantities the following three types of data:

$$\left\{h_t;\, D_i \le t \le D_i + \Delta_i\right\}, \tag{1.1}$$

which denote the altimetric observations (i.e., the height of the sea surface over the reference ellipsoid) collected along a track i during a period Δ_i, over the area of study A_S at date D_i; $\{\Delta g(P_i)\}$, which denote a set of free-air gravity anomalies in the area A_S; and observations of the anomalous potential $\{T_{ij}\}$ and of its second order derivatives $\{(T_{rr})_{ij}\}$ given on a sphere at mean satellite altitude at a point P_j along a track i, like those that can be derived from the GOCE mission employing the so called space-wise data analysis (Migliaccio *et al* 2004, 2006, 2007, submitted). The main tool that will be applied to perform a consistent combination of all data and predict the geoid and the quasi-stationary SST is an empirical analysis technique derived from the Wiener-Kolmogorov prediction theory, and referred to in geodetic literature as least squares collocation (LSC).

The first two data sets are the classical ones in geodetic literature and practice and have been used for long in the determination of gravity field functionals and quantities related to the marine geoid. Their combination schemes using collocation will be reviewed in §3. The use of the third type of data sets, namely of the disturbing potential and its second order derivatives at satellite level, and the study of their impact on the accuracy of the derived solutions, have been analytically studied in the frame of the Greek-Italian bilateral project and will be summarized in §4. Finally, considering that the aforementioned collocation technique, with its stepwise approach to the empirical estimation of covariances, can produce biases in the predicted quantities (Reguzzoni *et al.* 2005), a new proposal is developed that should enable us to make a better estimate of the second order solutions, i.e., the covariances, of the relevant fields. This proposal is developed and presented in §5, where the conclusions follow. In the next paragraph we shortly summarize the fundamentals of the observation equations of our data and of the collocation technique.

2 Observation equations and collocation

Let us start by recalling the form of the observation equations of our data with the understanding that in this section whenever we write the anomalous potential T we mean the anomalous potential already reduced by some preliminary global model, up to a medium degree, e.g., n=180 or n=200. First of all we have the following observation equation:

$$h_t = a_i + b_i(t - D_i) + N_t + \zeta_t + v_t\,, \tag{2.1}$$

where: a_i, b_i are the bias and tilt of the track i; N_t denotes the geoid height at the sub-satellite point P_t along track i; ζ_t denotes the quasi-stationary SST at the same point P_t; v_t is the (uncorrelated) noise of the observations.

Note that usually the model presented in Eq. 2.1 is augmented with the inclusion of an orbit error and some time dependant oceanic signal, e.g., tides. The orbit error stems from the fact that h_t is derived from the ellipsoidal height of the satellite minus the true observation, which is just the height of the satellite over the sea measured by radars. Of course the height of the satellite derived from tracking data contains an estimation error which however is nowadays reduced to very few centimeters (Le Traon *et al.* 1995, Le Traon and Ogor 1998, Schrama 1989). In any case, both signals are so smooth for a short track, like those present in the Mediterranean Sea, that they are known to be well represented by the linear trend term in Eq. 2.1. The rest of the time varying effects of the SST are absorbed by the error term of Eq. 2.1. It should be noted that the time-varying part of the SST can be regarded as a stationary random signal, therefore its contribution can be modeled and removed by the error/noise term of Eq. 2.1. As shown in Cazenave (2002), Fenoglio (2002), Larnicol *et al.* (1995) and Tziavos *et al.* (2005) the time varying sea surface topography in the Mediterranean Sea presents clear seasonal characteristics and one may object that it cannot be regarded as a random signal. Here we should distinguish two cases. The first one refers to the scheme described by Eq. 2.1 where we are dealing with a single altimetric track i. In this case, that the data span over a limited time period t, the time-varying (TSST) can be regarded as a random signal and be absorbed by the noise term. The second case is when a large amount of data is available spanning a large period of time, e.g., when a complete annual-cycle of exact repeat mission altimetry data are available. In this case, the signal of the TSST cannot be regarded as purely random, due to its (partly) seasonal characteristics. Nevertheless the bias term a introduced in Eq. 2.1 includes any TSST signal with non-random characteristics, and any remaining random part is absorbed by the noise term. A more complete representation of Eq. 2.1 is given in §3 where a dedicated variable $\delta\zeta$ is introduced to describe the TSST. Moreover, let us remark that the SST field described by ζ_t is quite small in the Mediterranean Sea reaching the 20 cm level as a maximum while the TSST is of the order of a few centimetres.

As for the other terms in Eq. 2.1 let us recall that the geoid height N is related to the disturbing potential T by Bruns' formula (Heiskanen and Moritz 1967)

$$N(P)=\frac{T(P)}{\gamma(P)}, \tag{2.2}$$

Note that in Eq. 2.2 when GPS/Levelling data are to be used, then the zero degree geoid term N_o should be added. The zero-degree term accounts in principle for the effects of mass and potential differences between the true geoid and the reference equipotential ellipsoid and appears as an offset between the EGM/gravimetric geoid heights and the geometric heights (Heiskanen and Moritz 1967). Free-air gravity anomalies Δg are given from the well-known fundamental equation of physical geodesy (ibid.)

$$\Delta g(P)=-\frac{\partial T(P)}{\partial h_P}-\frac{1}{\gamma(P)}\frac{\partial \gamma(P)}{\partial h_P}T(P), \tag{2.3}$$

Given that the normal to the earth ellipsoid is reasonably approximated by the direction of the radius vector r, Eq. 2.3 becomes

$$\Delta g(P)=-\frac{\partial T(P)}{\partial r_P}-\frac{1}{\gamma(P)}\frac{\partial \gamma(P)}{\partial r_P}T(P). \tag{2.4}$$

Notice that in Eqs. 2.3 and 2.4 the gravity anomalies are accompanied by a noise $v_{\Delta g}$ of the order of 5 mGals. Of course the gravity information represented by Eq. 2.4 can include airborne data as well as gravity disturbances either on land or at sea from altimetry inversion. Finally, T and T_{rr} (the second radial derivative) do not need to be written in terms of observation equations, since they are self-explanatory. We only observe that they are given at an altitude of, say, 200 km and that they are typically affected by errors in the range of $\sigma(T/\gamma)\sim 1\text{cm}$ and $\sigma(T_{rr})\sim 0.5\cdot 10^{-3}$ E.U. The common structure of these data is of utmost importance; we will not discuss it within this paper, we shall only assume that it has been derived in the GOCE data analysis framework (Migliaccio *et al.* 2007, Pail 2003, Rummel *et al.* 2004, Sünkel 2002). Now that the observation equations have been written, let us make the following hypothesis on the covariance structure of the different signals (N, ζ, T, T_{rr}) and noises involved (Knudsen 1987, Moritz 1980, Tscherning 1986, Tscherning 1993, Tscherning and Rapp 1974, Sansò 1986):

(i) T has an isotropic covariance function, with structure

$$C_{TT}(P,Q)=\left(\frac{GM}{R}\right)^2\sum_{n=0}^{n_{\max}}c_n(T)\left(\frac{R^2}{r_Q r_P}\right)^{n+1}P_n(\cos\psi_{PQ})+\left(\frac{GM}{R}\right)^2\sum_{n=n_{\max}+1}^{\infty}\sigma_n(T)\left(\frac{R_B^2}{r_Q r_P}\right)^{n+1}P_n(\cos\psi_{PQ}), \tag{2.5}$$

where, G is Newton's gravitational constant and M is the mass of the Earth, $c_n(T)$ are degree variances up to the full power of the reference model, R_B is the so-called radius of the Bjerhammar sphere, P_n are the non-normalized Legendre polynomials, $\sigma_n(T)$ are the degree variances adopted above the maximum degree of expansion until infinity according to the model of Tscherning and Rapp (1974) (see also §4);

(ii) given Eqs. 2.4 and 2.5 and by covariance propagation we have the auto-covariance functions for geoid heights, gravity anomalies and the second order derivatives of the disturbing potential

$$C_{NN}(P,Q)=\frac{1}{\gamma_P\gamma_Q}C_{TT}(P,Q), \tag{2.6}$$

$$\begin{aligned}C_{\Delta g\Delta g}(P,Q)=&\left(\frac{GM}{R}\right)^2\sum_{n=0}^{n_{\max}}(n-1)^2c_n(T)\left(\frac{R^2}{r_Q r_P}\right)^{n+2}P_n(\cos\psi_{PQ})+\\&+\left(\frac{GM}{R}\right)^2\sum_{n=n_{\max}+1}^{\infty}(n-1)^2\sigma_n(T)\left(\frac{R_B^2}{r_Q r_P}\right)^{n+2}P_n(\cos\psi_{PQ})\end{aligned}, \tag{2.7}$$

$$C_{T_{rr}T_{rr}}\left(P,Q\right)=\left(\frac{GM}{R^3}\right)^2\sum_{n=0}^{n_{\max}}\left(n+1\right)^2\left(n+2\right)^2 c_n\left(T\right)\left(\frac{R^2}{r_Q r_P}\right)^{n+3}P_n\left(\cos\psi_{PQ}\right)+$$
$$+\left(\frac{GM}{R^3}\right)^2\sum_{n=n_{\max}+1}^{\infty}\left(n+1\right)^2\left(n+2\right)^2\sigma_n\left(T\right)\left(\frac{R_B^2}{r_Q r_P}\right)^{n+3}P_n\left(\cos\psi_{PQ}\right) \quad (2.8)$$

In the same way we can define all the appropriate cross-covariance functions such as $C_{\Delta gT}, C_{\Delta gN}, C_{TN}, C_{T_{rr}T}, C_{\Delta gT_{rr}}$, and $C_{T_{rr}N}$

$$C_{\Delta gT}\left(P,Q\right)=\frac{GM^2}{R^3}\sum_{n=0}^{n_{\max}}\left(n-1\right)c_n\left(T\right)\left(\frac{R}{r_P}\right)^{n+2}\left(\frac{R}{r_Q}\right)^{n+1}P_n\left(\cos\psi_{PQ}\right)+$$
$$+\frac{GM^2}{R^3}\sum_{n=n_{\max}+1}^{\infty}\left(n-1\right)\sigma_n\left(T\right)\left(\frac{R_B}{r_P}\right)^{n+2}\left(\frac{R_B}{r_Q}\right)^{n+1}P_n\left(\cos\psi_{PQ}\right) \quad (2.9)$$

$$C_{\Delta gN}\left(P,Q\right)=\frac{1}{\gamma_Q}C_{\Delta gT}\left(P,Q\right), \quad (2.10)$$

$$C_{TN}\left(P,Q\right)=\frac{1}{\gamma_Q}C_{TT}\left(P,Q\right), \quad (2.11)$$

$$C_{T_{rr}T}\left(P,Q\right)=\frac{GM^2}{R^4}\sum_{n=0}^{n_{\max}}\left(n+1\right)\left(n+2\right)c_n\left(T\right)\left(\frac{R}{r_P}\right)^{n+3}\left(\frac{R}{r_Q}\right)^{n+1}P_n\left(\cos\psi_{PQ}\right)+$$
$$+\frac{GM^2}{R^4}\sum_{n=0}^{n_{\max}}\left(n+1\right)\left(n+2\right)\sigma_n\left(T\right)\left(\frac{R_B}{r_P}\right)^{n+3}\left(\frac{R_B}{r_Q}\right)^{n+1}P_n\left(\cos\psi_{PQ}\right) \quad (2.12)$$

$$C_{\Delta gT_{rr}}\left(P,Q\right)=\frac{GM^2}{R^5}\sum_{n=0}^{n_{\max}}\left(n-1\right)\left(n+1\right)\left(n+2\right)c_n\left(T\right)\left(\frac{R}{r_P}\right)^{n+2}\left(\frac{R}{r_Q}\right)^{n+3}P_n\left(\cos\psi_{PQ}\right)+$$
$$+\frac{GM^2}{R^5}\sum_{n=0}^{n_{\max}}\left(n-1\right)\left(n+1\right)\left(n+2\right)\sigma_n\left(T\right)\left(\frac{R_B}{r_P}\right)^{n+2}\left(\frac{R_B}{r_Q}\right)^{n+3}P_n\left(\cos\psi_{PQ}\right) \quad (2.13)$$

$$C_{T_{rr}N}\left(P,Q\right)=\frac{1}{\gamma_Q}C_{T_{rr}T}\left(P,Q\right). \quad (2.14)$$

Note that in Eqs. 2.6-2.14 when, e.g., $C_{T_{rr}N}\left(P,Q\right)$ is derived, it is assumed that T_{rr} refers to point P and N to point Q.

(iii) v_t is a noise with given variance;
(iv) $v_{\Delta g}$ is a noise with given variance;
(v) v_T and $v_{T_{rr}}$ are prediction errors of T and T_{rr}, with given covariance and cross-covariance structure;
(vi) the noises in (iii), (iv) and (v) are independent from one another and independent from T;
(vii) ζ_t has some (unknown) isotropic covariance in A_S;
(viii) ζ_t is independent of T and of all noises.

Given all the aforementioned equations, we can compact our observation equation (see Eq. 2.1) in the following form (Moritz, 1980):

$$\mathbf{y}=\mathbf{A}\mathbf{x}+\mathbf{s}+\mathbf{v}, \quad (2.15)$$

where the bold-faced symbols denote vectors or matrices. In Eq. 2.15, ***y*** is the full observation vector, that contains the along track sea surface height observations ***h***, the available marine gravity anomalies ***Δg*** at sparse points on the surface, and the disturbing potential and its second order derivatives data on grids at satellite level coming from GOCE-like missions, i.e., $\boldsymbol{T}^{os}$ and $\boldsymbol{T}_{rr}^{os}$. Therefore, the data vector can be written as:

$$\mathbf{y} = \begin{bmatrix} \mathbf{h}^T & \Delta\mathbf{g}^T & \mathbf{T}^{\mathbf{os}^T} & \mathbf{T}_{\mathbf{rr}}^{\mathbf{os}^T} \end{bmatrix}^T, \tag{2.16}$$

Moreover, in Eq. 2.15, ***x*** is the vector of the unknown deterministic parameters describing the bias and tilt of the *N* altimetric tracks considered:

$$\mathbf{x} = \begin{bmatrix} \dots \\ a_i \\ b_i \\ \dots \end{bmatrix} \quad i = 1, 2, ..., N, \tag{2.17}$$

and ***A*** is the design matrix of our observation equations describing the influence of the parameters ***x*** on the signal in ***y***. Equivalently, ***s*** is the set of signals,

$$\mathbf{s} = \begin{bmatrix} \frac{1}{\gamma}\mathbf{T} + \zeta \\ -\frac{\partial \mathbf{T}}{\partial r} - \frac{2}{r}\mathbf{T} \\ \mathbf{T}^{\mathbf{S}} \\ \mathbf{T}_{\mathbf{rr}}^{\mathbf{S}} \end{bmatrix} = \begin{bmatrix} \frac{1}{\gamma}\mathbf{T} + \zeta \\ -\mathbf{T}_r - \frac{2}{r}\mathbf{T} \\ \mathbf{T}^{\mathbf{S}} \\ \mathbf{T}_{\mathbf{rr}}^{\mathbf{S}} \end{bmatrix}, \tag{2.18}$$

where all of its components, i.e., $\frac{1}{\gamma}\mathbf{T} + \zeta, -\mathbf{T}_r - \frac{2}{r}\mathbf{T}, \mathbf{T}^{\mathbf{S}}, \mathbf{T}_{\mathbf{rr}}^{\mathbf{S}}$, must be consistently related through one and the same covariance function. Finally, ***v*** is the vector of noises and estimation errors, with the covariance properties illustrated by (iii), (iv), (v) and (vi) above:

$$\nu = \begin{bmatrix} \nu_t \\ \nu_{\Delta g} \\ \nu_T \\ \nu_{T_{rr}} \end{bmatrix}. \tag{2.19}$$

If we assume to know $\mathbf{C}_{TT}(P,Q)$, $\mathbf{C}_{\zeta\zeta}(P,Q)$ and $\mathbf{C}_{T\zeta}(P,Q)$, that is the covariance and cross-covariance functions of the disturbing potential and of the sea surface topography, then with the further assumption (viii) listed above, we can construct the full variance-covariance matrix of both $\mathbf{s}$ and $\mathbf{v}$, i.e.,

$$\mathbf{C}_{yy} = \mathbf{C}_{ss} + \mathbf{C}_{vv}, \tag{2.20}$$

As well as all the cross-covariance functions like

$$\mathbf{C}_{Ty}(P,Q) = \mathbf{C}_{Ts}(P,Q), \tag{2.21}$$

$$\mathbf{C}_{\zeta y}(P,Q) = \mathbf{C}_{\zeta s}(P,Q), \tag{2.22}$$

Now we can perform the optimal linear estimate of $\mathbf{x}$, and the prediction of $T(P)$ and $\zeta(P)$ for any given point *P*, analytically according to the formulas (Knudsen 1987, 1993)

$$\hat{\mathbf{x}} = \left(\mathbf{A}^T\mathbf{C}_{yy}^{-1}\mathbf{A}\right)\mathbf{A}^T\mathbf{C}_{yy}^{-1}\mathbf{y}, \tag{2.23}$$

$$\hat{T}(P) = \mathbf{C}_{Ts}(P,\cdot)\mathbf{C}_{yy}^{-1}(\mathbf{y} - \mathbf{A}\hat{\mathbf{x}}), \tag{2.24}$$

$$\hat{\zeta}(P) = \mathbf{C}_{\zeta s}(P,\cdot)\mathbf{C}_{yy}^{-1}(\mathbf{y} - \mathbf{A}\hat{\mathbf{x}}). \tag{2.25}$$

Also, prediction errors of both $\hat{T}(P)$ and $\hat{\zeta}(P)$ can be computed, at least in principle, from

$$\sigma_{\mathrm{T}}^2(P) = \mathbf{C}_{TT}(P,P) - \mathbf{C}_{Ts}\left\{\mathbf{C}_{yy}^{-1} - \mathbf{C}_{yy}^{-1}\mathbf{A}\mathbf{N}^{-1}\mathbf{A}^T\mathbf{C}_{yy}^{-1}\right\}\mathbf{C}_{sT}, \tag{2.26}$$

$$\sigma_{\zeta}^2(P) = \mathbf{C}_{\zeta\zeta}(P,P) - \mathbf{C}_{\zeta s}\left\{\mathbf{C}_{yy}^{-1} - \mathbf{C}_{yy}^{-1}\mathbf{A}\mathbf{N}^{-1}\mathbf{A}^T\mathbf{C}_{yy}^{-1}\right\}\mathbf{C}_{s\zeta}. \tag{2.27}$$

In order to implement an estimation scheme like the one described previously, we have to face two difficulties: a) to understand where one can get the covariances of T and in particular the local covariances, as well as that of ζ and b) the unequivocal complexity arising from the need of solving systems of the same dimensions as $\boldsymbol{y}$. In the next two paragraphs we shall see how this has been done in past and recent studies.

3 Heterogeneous data combination for gravity field and sea surface topography modelling

3.1 Spectral domain heterogeneous data combination for gravity field modelling

Having outlined the LSC based heterogeneous data combination in the previous section, its frequency domain representation will be presented here, while a specific example of gravimetric, altimetric and GOCE potential and second order differences data combination for geoid determination will be given. Moreover, the similarities and differences between system theory and LSC are outlined, in order to show the physical relation between all methods presented in this work. The second part of this section is devoted to an outline of mean dynamic topography determination using LSC.

Since the beginning of the 80's, spectral methods and FT in particular, have been extensively used for the solution of the classical boundary value problems of physical geodesy. The key concept for the utilization of FT in geodetic problems lays to the representation of well-known integral formulas (e.g., Stokes' and Vening-Meinesz integrals for the prediction of geoid heights from gravity anomalies and deflections of the vertical, respectively) as convolution integrals. Since, in the spectral domain the convolution of input signals is replaced by simple multiplication of their spectra, FT and Fast Fourier Transforms (FFT) have been used mainly due to their high-efficiency in terms of time, compared to the usual integral methods of solving geodetic boundary value problems (Tziavos *et al.* 1998a,b; Vergos *et al.* 2005a,b). Despite the gain in processing time, FFT methods carry some disadvantages, among which the main ones are: a) The need for regularly spaced (i.e., gridded) data, b) the inability of predicting the estimation error for the output signal (Andritsanos *et al*. 2001, Sideris 1996, Sansò & Sideris 1997) and c) the prerequisite of having a single input and a single output signal. On the other hand, the leading estimation method in physical geodesy, i.e., LSC, which was previously discussed in the frame of heterogeneous data combination schemes, allows the use of multiple input signals and irregularly distributed data, while it provides an optimal, under the Wiener-Kolmogorov principle, estimate of the output signal with simultaneous estimation of the full variance-covariance matrix of the output signal error (Moritz 1980). As it was shown in the previous section, in contrast to FT and FFT methods, LSC can incorporate multiple sources of heterogeneous input data if their covariance and auto-covariance functions have been computed. A nice discussion on the a-priori estimation of error covariance functions is given in Arabelos *et al*. (2007).

Nevertheless, especially in modern day geodetic applications with the hundreds of thousands of altimetric, gravimetric and space borne gravity field related observations, the application of LSC has become difficult. Therefore, a frequency domain equivalent to LSC has been developed employing system theory. The latter has been traditionally used in signal processing and signal transmission methods as well as to various applications of electrical engineering. Sideris (1996) was the first one who proposed a solution of geodetic boundary value problems in the frequency domain employing system theory and presenting the general scheme for the use of a system with multiple inputs and multiple outputs (Multiple Input Multiple Output System Theory – MIMOST). Numerical solutions and examples of using MIMOST methods for the estimation of geoid heights, gravity anomalies, deflections of the vertical, the quasi-stationary sea surface topography from heterogeneous noisy data as well as in combined gravimetric and GPS geoid solutions have been presented in several papers (see, e.g., Andritsanos 2000; Andritsanos et al. 2001, 2004; Andritsanos and Tziavos 2002; Vergos et al. 2005).

Let us assume that gravity, altimetry and GOCE observations, i.e., potential and its second order radial derivatives, are available with the aim of predicting geoid heights, then a MIMOST system with four input

signals and a single output will look like the flowchart presented in Figure 1. In the system presented in Fig. 1 we have four input signals, $\boldsymbol{N}^{gr}$, $\boldsymbol{N}^{alt}$, $\boldsymbol{T}^{GOCE}$, and $\boldsymbol{T}_{rr}^{GOCE}$ which are contaminated by noise $\boldsymbol{m}^{gr}$, $\boldsymbol{m}^{alt}$, $\boldsymbol{m}_{T}^{GOCE}$ and $\boldsymbol{m}_{T_{rr}}^{GOCE}$ in order to simulate their errors. Moreover what we really know are just the variances and not the complete errors of the signal. Nevertheless, it should be noted that as shown by Andritsanos et al. (2001) in the case of exact repeat altimetric missions an estimation of the input error Power Spectral Density (PSD) function can be directly evaluated using this successive information.

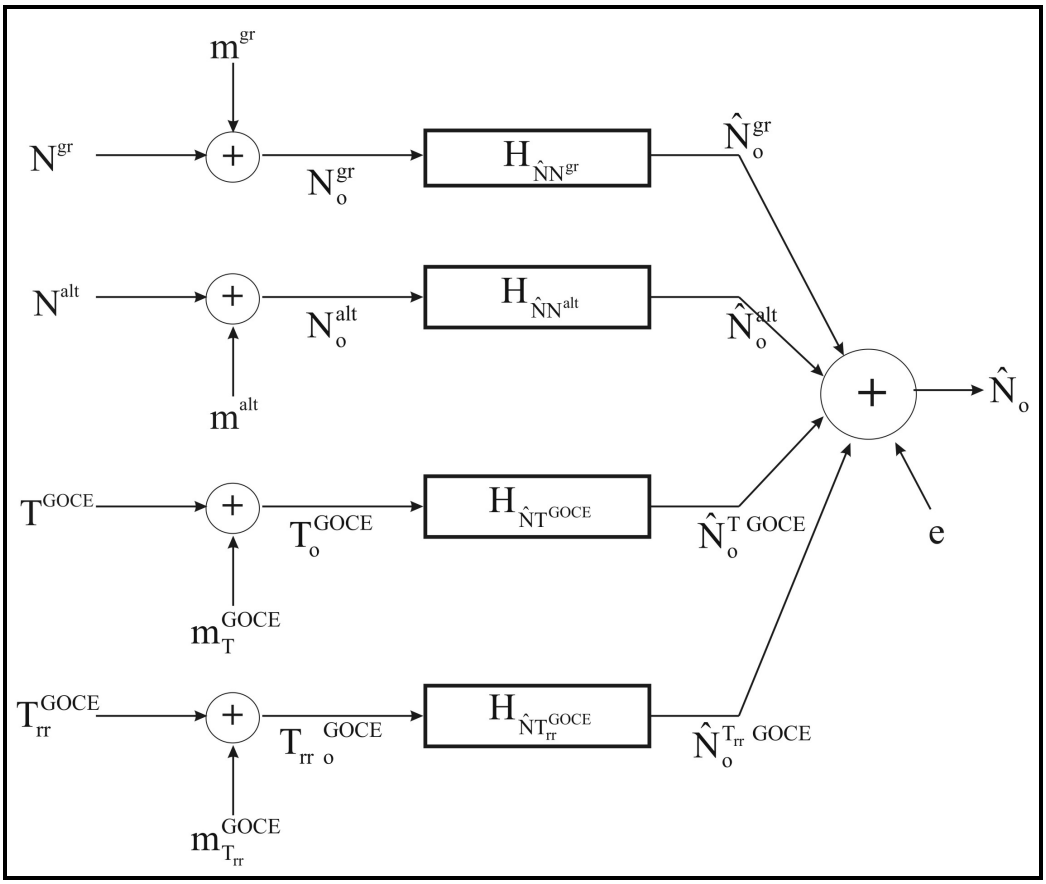

Figure 1: A quad-input single output system for the prediction of geoid heights from gravity, altimetry and GOCE data.

The final solutions and the error PSD function of the MIMOST method are calculated according to the following equations (*ibid.*, Sideris 1996):

$$\hat{\mathbf{N}}_o = \begin{bmatrix} \mathbf{H}_{\hat{N}N^{gr}} & \mathbf{H}_{\hat{N}N^{alt}} & \mathbf{H}_{\hat{N}T^{GOCE}} & \mathbf{H}_{\hat{N}T_{rr}^{GOCE}} \end{bmatrix} \left(\begin{bmatrix} \mathbf{P}_{N_o^{gr}N_o^{gr}} & \mathbf{P}_{N_o^{gr}N_o^{alt}} & \mathbf{P}_{N_o^{gr}T_o^{GOCE}} & \mathbf{P}_{N_o^{gr}T_{rr\,o}^{GOCE}} \\ \mathbf{P}_{N_o^{alt}N_o^{gr}} & \mathbf{P}_{N_o^{alt}N_o^{alt}} & \mathbf{P}_{N_o^{alt}T_o^{GOCE}} & \mathbf{P}_{N_o^{alt}T_{rr\,o}^{GOCE}} \\ \mathbf{P}_{T_o^{GOCE}N_o^{gr}} & \mathbf{P}_{T_o^{GOCE}N_o^{alt}} & \mathbf{P}_{T_o^{GOCE}T_o^{GOCE}} & \mathbf{P}_{T_o^{GOCE}T_{rr\,o}^{GOCE}} \\ \mathbf{P}_{T_{rr\,o}^{GOCE}N_o^{gr}} & \mathbf{P}_{T_{rr\,o}^{GOCE}N_o^{alt}} & \mathbf{P}_{T_{rr\,o}^{GOCE}T_o^{GOCE}} & \mathbf{P}_{T_{rr\,o}^{GOCE}T_{rr\,o}^{GOCE}} \end{bmatrix} - \right.$$

$$\left. - \begin{bmatrix} \mathbf{P}_{m^{gr}m^{gr}} & 0 & 0 & 0 \\ 0 & \mathbf{P}_{m^{alt}m^{alt}} & 0 & 0 \\ 0 & 0 & \mathbf{P}_{m_T^{GOCE}m_T^{GOCE}} & 0 \\ 0 & 0 & 0 & \mathbf{P}_{m_{T_{rr}}^{GOCE}m_{T_{rr}}^{GOCE}} \end{bmatrix} \right) \left(\begin{bmatrix} \mathbf{P}_{N_o^{gr}N_o^{gr}} & \mathbf{P}_{N_o^{gr}N_o^{alt}} & \mathbf{P}_{N_o^{gr}T_o^{GOCE}} & \mathbf{P}_{N_o^{gr}T_{rr\,o}^{GOCE}} \\ \mathbf{P}_{N_o^{alt}N_o^{gr}} & \mathbf{P}_{N_o^{alt}N_o^{alt}} & \mathbf{P}_{N_o^{alt}T_o^{GOCE}} & \mathbf{P}_{N_o^{alt}T_{rr\,o}^{GOCE}} \\ \mathbf{P}_{T_o^{GOCE}N_o^{gr}} & \mathbf{P}_{T_o^{GOCE}N_o^{alt}} & \mathbf{P}_{T_o^{GOCE}T_o^{GOCE}} & \mathbf{P}_{T_o^{GOCE}T_{rr\,o}^{GOCE}} \\ \mathbf{P}_{T_{rr\,o}^{GOCE}N_o^{gr}} & \mathbf{P}_{T_{rr\,o}^{GOCE}N_o^{alt}} & \mathbf{P}_{T_{rr\,o}^{GOCE}T_o^{GOCE}} & \mathbf{P}_{T_{rr\,o}^{GOCE}T_{rr\,o}^{GOCE}} \end{bmatrix} \right)^{-1} \begin{bmatrix} \mathbf{N}_o^{gr} \\ \mathbf{N}_o^{alt} \\ \mathbf{T}_o^{GOCE} \\ \mathbf{T}_{rr\,o}^{GOCE} \end{bmatrix} \quad , \qquad (3.1)$$

$$
\begin{aligned}
\mathbf{P}_{\hat{e}\hat{e}} = \Bigg\{ & \begin{bmatrix} \mathbf{H}_{\hat{N}N^{gr}} & \mathbf{H}_{\hat{N}N^{alt}} & \mathbf{H}_{\hat{N}T^{GOCE}} & \mathbf{H}_{\hat{N}T_{rr}^{GOCE}} \end{bmatrix} \Bigg(\begin{bmatrix} \mathbf{P}_{N_o^{gr}N_o^{gr}} & \mathbf{P}_{N_o^{gr}N_o^{alt}} & \mathbf{P}_{N_o^{gr}T_o^{GOCE}} & \mathbf{P}_{N_o^{gr}T_{rr\,o}^{GOCE}} \\ \mathbf{P}_{N_o^{alt}N_o^{gr}} & \mathbf{P}_{N_o^{alt}N_o^{alt}} & \mathbf{P}_{N_o^{alt}T_o^{GOCE}} & \mathbf{P}_{N_o^{alt}T_{rr\,o}^{GOCE}} \\ \mathbf{P}_{T_o^{GOCE}N_o^{gr}} & \mathbf{P}_{T_o^{GOCE}N_o^{alt}} & \mathbf{P}_{T_o^{GOCE}T_o^{GOCE}} & \mathbf{P}_{T_o^{GOCE}T_{rr\,o}^{GOCE}} \\ \mathbf{P}_{T_{rr\,o}^{GOCE}N_o^{gr}} & \mathbf{P}_{T_{rr\,o}^{GOCE}N_o^{alt}} & \mathbf{P}_{T_{rr\,o}^{GOCE}T_o^{GOCE}} & \mathbf{P}_{T_{rr\,o}^{GOCE}T_{rr\,o}^{GOCE}} \end{bmatrix} - \\
& - \begin{bmatrix} \mathbf{P}_{m^{gr}m^{gr}} & 0 & 0 & 0 \\ 0 & \mathbf{P}_{m^{alt}m^{alt}} & 0 & 0 \\ 0 & 0 & \mathbf{P}_{m_T^{GOCE}m_T^{GOCE}} & 0 \\ 0 & 0 & 0 & \mathbf{P}_{m_{Trr}^{GOCE}m_{Trr}^{GOCE}} \end{bmatrix} \Bigg) - \\
& - \begin{bmatrix} \hat{\mathbf{H}}_{\hat{N}N^{gr}} & \hat{\mathbf{H}}_{\hat{N}N^{alt}} & \hat{\mathbf{H}}_{\hat{N}T^{GOCE}} & \hat{\mathbf{H}}_{\hat{N}T_{rr}^{GOCE}} \end{bmatrix} \begin{bmatrix} \mathbf{P}_{N_o^{gr}N_o^{gr}} & \mathbf{P}_{N_o^{gr}N_o^{alt}} & \mathbf{P}_{N_o^{gr}T_o^{GOCE}} & \mathbf{P}_{N_o^{gr}T_{rr\,o}^{GOCE}} \\ \mathbf{P}_{N_o^{alt}N_o^{gr}} & \mathbf{P}_{N_o^{alt}N_o^{alt}} & \mathbf{P}_{N_o^{alt}T_o^{GOCE}} & \mathbf{P}_{N_o^{alt}T_{rr\,o}^{GOCE}} \\ \mathbf{P}_{T_o^{GOCE}N_o^{gr}} & \mathbf{P}_{T_o^{GOCE}N_o^{alt}} & \mathbf{P}_{T_o^{GOCE}T_o^{GOCE}} & \mathbf{P}_{T_o^{GOCE}T_{rr\,o}^{GOCE}} \\ \mathbf{P}_{T_{rr\,o}^{GOCE}N_o^{gr}} & \mathbf{P}_{T_{rr\,o}^{GOCE}N_o^{alt}} & \mathbf{P}_{T_{rr\,o}^{GOCE}T_o^{GOCE}} & \mathbf{P}_{T_{rr\,o}^{GOCE}T_{rr\,o}^{GOCE}} \end{bmatrix} \Bigg\} \\
& \left(\begin{bmatrix} \mathbf{H}^{\dagger}_{\hat{N}N^{gr}} \\ \mathbf{H}^{\dagger}_{\hat{N}N^{alt}} \\ \mathbf{H}^{\dagger}_{\hat{N}T^{GOCE}} \\ \mathbf{H}^{\dagger}_{\hat{N}T_{rr}^{GOCE}} \end{bmatrix} - \begin{bmatrix} \hat{\mathbf{H}}^{\dagger}_{\hat{N}N^{gr}} \\ \hat{\mathbf{H}}^{\dagger}_{\hat{N}N^{alt}} \\ \hat{\mathbf{H}}^{\dagger}_{\hat{N}T^{GOCE}} \\ \hat{\mathbf{H}}^{\dagger}_{\hat{N}T_{rr}^{GOCE}} \end{bmatrix} \right)^{\dagger} + \begin{bmatrix} \hat{\mathbf{H}}_{\hat{N}N^{gr}} & \hat{\mathbf{H}}_{\hat{N}N^{alt}} & \hat{\mathbf{H}}_{\hat{N}T^{GOCE}} & \hat{\mathbf{H}}_{\hat{N}T_{rr}^{GOCE}} \end{bmatrix} \\
& \begin{bmatrix} \mathbf{P}_{m^{gr}m^{gr}} & 0 & 0 & 0 \\ 0 & \mathbf{P}_{m^{alt}m^{alt}} & 0 & 0 \\ 0 & 0 & \mathbf{P}_{m_T^{GOCE}m_T^{GOCE}} & 0 \\ 0 & 0 & 0 & \mathbf{P}_{m_{Trr}^{GOCE}m_{Trr}^{GOCE}} \end{bmatrix} \begin{bmatrix} \hat{\mathbf{H}}^{\dagger}_{\hat{N}N^{gr}} \\ \hat{\mathbf{H}}^{\dagger}_{\hat{N}N^{alt}} \\ \hat{\mathbf{H}}^{\dagger}_{\hat{N}T^{GOCE}} \\ \hat{\mathbf{H}}^{\dagger}_{\hat{N}T_{rr}^{GOCE}} \end{bmatrix} \qquad . \qquad (3.2)
\end{aligned}
$$

In Eqs. 3.1 and 3.2 $\hat{N}_o$ is the combined geoid estimation, N^{gr}, N^{alt}, T^{GOCE} and T_{rr}^{GOCE} are the pure gravimetric, altimetric, GOCE potential and second order derivatives signals, respectively, N_o^{gr}, N_o^{alt}, T_o^{GOCE} and $T_{o\ rr}^{\ GOCE}$ are the gravimetric, altimetric, GOCE potential and second order derivatives observations, m^{gr}, m^{alt}, m_T^{GOCE} and $m_{T_{rr}}^{GOCE}$ are the input noises of the gravity anomaly, altimetric sea surface heights, potential and second order derivatives input signals respectively, H_{xy} is the theoretical operator that connects the pure input and output signals, $\hat{\mathbf{H}}_{x_o y_o}$ is the optimum frequency impulse response function, $\mathbf{P}_{\hat{e}\hat{e}}$ is the error PSD function, e is the noise of the output signal and the † denotes the adjoint, i.e., the transpose, complex conjugate of the matrix under consideration.

If we substitute the vector of observation and estimation signals with

$$
\mathbf{Y}_o = \begin{bmatrix} \mathbf{N}_o^{gr} \\ \mathbf{N}_o^{alt} \\ \mathbf{T}_o^{GOCE} \\ \mathbf{T}_{rr\ o}^{\ GOCE} \end{bmatrix}; \quad \mathbf{X}_o = \left[N_o \right], \qquad (3.3)
$$

then Eqs. 3.1 and 3.2 can be written in matrix notation as

$$
\hat{\mathbf{X}}_o = \hat{\mathbf{H}}_{X_o Y_o} \mathbf{Y}_o = \mathbf{P}_{XY} \mathbf{P}_{Y_o Y_o}^{-1} \mathbf{Y}_o = \mathbf{H}_{XY} \left(\mathbf{P}_{Y_o Y_o} - \mathbf{P}_{mm} \right) \mathbf{P}_{Y_o Y_o}^{-1} \mathbf{Y}_o , \qquad (3.4)
$$

$$
\mathbf{P}_{\hat{e}\hat{e}} = \left[\mathbf{H}_{XY} \left(\mathbf{P}_{Y_o Y_o} - \mathbf{P}_{mm} \right) - \hat{\mathbf{H}}_{X_o Y_o} \mathbf{P}_{Y_o Y_o} \right] \left(\mathbf{H}_{XY}^{*T} - \hat{\mathbf{H}}_{X_o Y_o}^{*T} \right) + \hat{\mathbf{H}}_{X_o Y_o} \mathbf{P}_{mm} \mathbf{H}_{XY}^{*T} , \qquad (3.5)
$$

where the theoretical operator impulse response function is

$$
\mathbf{H}_{XY} = \mathbf{P}_{XY} \mathbf{P}_{YY}^{-1} . \qquad (3.6)
$$

In order to see the equivalence of MIMOST with space domain least squares collocation, let us assume that we have a stationary, isotropic random input signal described by the vector

$$\mathbf{y} = \begin{bmatrix} \mathbf{N}_o^{gr} \\ \mathbf{N}_o^{alt} \\ \mathbf{T}_o^{GOCE} \\ \mathbf{T}_{rr\ o}^{GOCE} \end{bmatrix}, \tag{3.7}$$

and that there exists a linear estimator ***h(x,y)*** (represented by ***h*** for simplicity) which relates the input signal ***y*** with the output signal ***x***, i.e.,

$$\mathbf{x}=\mathbf{h}\mathbf{y}. \tag{3.8}$$

If we denote the error vector by ***e*** then its covariance matrix will be given as:

$$\mathbf{C}_{\hat{e}\hat{e}} = E\left\{\mathbf{e}\mathbf{e}^{\mathrm{T}}\right\} = \mathbf{h}E\left\{\mathbf{Y}\mathbf{Y}^{\mathrm{T}}\right\}\mathbf{h}^{\mathrm{T}} - E\left\{\mathbf{X}\mathbf{Y}^{\mathrm{T}}\right\}\mathbf{h}^{\mathrm{T}} - \mathbf{h}E\left\{\mathbf{Y}\mathbf{X}^{\mathrm{T}}\right\} + E\left\{\mathbf{X}\mathbf{X}^{\mathrm{T}}\right\}, \tag{3.9}$$

where $E\{\cdot\}$ denotes expectation. From Eq. 3.9, taking into account that all our signals are centered ($E\{\cdot\}=0$) and that $\boldsymbol{C}_{(\cdot)(\cdot)} = E\{(\cdot)(\cdot)^T\}$, after some simple algebra we arrive at the following expression for the error covariance matrix of the output signal

$$\mathbf{C}_{\hat{e}\hat{e}} = \mathbf{C}_{XX} - \mathbf{C}_{XY}\mathbf{C}_{YY}^{-1}\mathbf{C}_{YX} + \left(\mathbf{h} - \mathbf{C}_{XY}\mathbf{C}_{YY}^{-1}\right)\mathbf{C}_{YY}\left(\mathbf{h} - \mathbf{C}_{XY}\mathbf{C}_{YY}^{-1}\right)^{T}. \tag{3.10}$$

Eq. 3.10 shows that the error covariance matrix of the predicted signal is composed by two parts, one that depends on the linear operator ***h*** (let us denote it as $\mathbf{A}_2 = \left(\mathbf{h} - \mathbf{C}_{XY}\mathbf{C}_{YY}^{-1}\right)\mathbf{C}_{YY}\left(\mathbf{h} - \mathbf{C}_{XY}\mathbf{C}_{YY}^{-1}\right)^{T}$) and another one that is independent of ***h*** (let us denote it as $\mathbf{A}_1 = \mathbf{C}_{XX} - \mathbf{C}_{XY}\mathbf{C}_{YY}^{-1}\mathbf{C}_{YX}$). The latter means that matrix $\boldsymbol{A_1}$ does not change for every possible linear prediction and every possible linear operator ***h***. According to Moritz (1980) in order to achieve the best unbiased minimum variance linear estimation of signal ***X*** from ***Y***, the matrix $\boldsymbol{A_2}$ should be put to zero, which holds if our linear operator is given as

$$\mathbf{h} = \mathbf{C}_{XY}\mathbf{C}_{YY}^{-1}. \tag{3.11}$$

Comparing Eqs. 3.6 and 3.11 we can easily verify that they are in fact the same with $\boldsymbol{h}(\mathrm{x},\mathrm{y}) \xrightarrow{\mathscr{F}} \boldsymbol{H}_{\mathrm{XY}}$, i.e., that ***h*** and $\boldsymbol{H}_{XY}$ form a FT pair. Given that, and comparing Eqs. 3.5 and 3.10 we can easily conclude on the similarity between MIMOST and LSC. An extensive presentation of LSC and MIMOST, as well as a detailed comparison between the two methods and a discussion on their similarities and differences is given in Sansò and Sideris (1997).

3.2 Heterogeneous data combination for sea surface topography modelling

One of the main problems in utilizing altimetric observations, i.e., heights of the sea surface above a reference ellipsoid acquired by radars on-board satellites, for marine geoid modeling, is that they refer to the instantaneous sea surface or after a reduction to the mean sea surface and not the geoid itself. In order to use altimetric sea surface heights (SSHs) in geoid determination it is mandatory to reduce them to the geoid, i.e., to remove the contribution of the sea surface topography and more particularly of its quasi-stationary part (also called mean dynamic topography – MDT). The main difficulty, as it will be outlined in the next section, comes from the fact that the available MDT models contain large errors close to the coastline, while in closed sea areas they are more or less inadequate due to the scarcity of available observations. It is worth mentioning that extensive efforts have been put during the last years for the use of altimetric data close to the coastline, especially through dedicated retracking of the original SSHs (see, e.g., Hwang *et al.* 2006, Kingdon *et al.* 2008, Madsen *et al.* 2007 and the references cited there). These offer a great potential for the determination of more accurate (at least close to the achievable accuracy in open oceans) MDT models. LSC offers a good opportunity to estimate both the quasi-stationary and the time-varying part of the sea surface topography in a combined adjustment scheme providing in this way rigorous MDT models for use in other studies. This, together with the derivation of covariance and cross-covariance functions for the geostrophic current velocities, will be discussed herein.

Let us assume that an altimetric observation can be described, in accordance to Eq. 2.1, with the following formula:

$$h = N + \zeta^c + \delta\zeta + v\,, \tag{3.12}$$

where:

N denotes the geoid height;
ζ^c denotes the quasi-stationary SST;
$\delta\zeta$ denotes the time-varying SST;
v is the (uncorrelated) noise of the observations.

If we further assume that a reference model to degree n_{max} is used, then the geoid covariance function is given by the formula 2.5, where we take:

$$c_n = \sum_{m=0}^{n}\left(C_{nm}^2 + S_{nm}^2\right),\ \sigma_n = \frac{a}{(n-1)(n-2)(n+24)} \tag{3.13}$$

moreover $\mathbf{C}_{NN} = \mathbf{C}_{TT}/\gamma^2$. In complete analogy to the geoid height covariance function, a similar kernel function associated with the MDT can be used to describe the statistical characteristics of the sea surface topography, i.e., (Knudsen and Tscherning, 2006):

$$\mathbf{C}_{\zeta^c\zeta^c} = \sum_{n=0}^{\infty}\left(\sigma_n^{\zeta}\right)\left(\frac{R_B}{R}\right)^{2(n+1)} P_n\left(\cos\psi\right). \tag{3.14}$$

Note that in LSC the analytical covariance function models should agree to the empirical values available for the area under study in order to represent the local statistical characteristics of the signal under consideration, i.e., the MDT in this case (Knudsen, 1991). For the description of the behaviour of the degree variances given in Eq. 3.14, Knudsen (1987, 1991, 1992, 1993) and Knudsen and Tscherning (2006) use a 3rd degree Butterworth filter so that the degree variances of the MDT are given as:

$$\left(\sigma_n^{\zeta^c}\right) = b\left(\frac{k_2^3}{k_2^3 + n^3} - \frac{k_1^3}{k_1^3 + n^3}\right). \tag{3.15}$$

with $b > 0$, $k_2 > k_1$. Note that in Eqs. 3.14 and 3.15 the factors b, k_1, k_2 and R_B are determined so that the analytic model fits the empirical values describing the statistical characteristics of the MDT in the area under study and more precisely the variance and the correlation length. In Knudsen (1991) the reference MDT used was based on a harmonic expansion of the Levitus permanent SST performed by Engelis (1987). The degree variances of that model reached maximum values at degrees 2 to 3 and decayed very fast to zero at degree 10 (corresponding to ~1800 km). Therefore, a Wiener-type of filtering function has been applied, based on Kaula's rule of thumb for the decay of the geoid power spectrum, i.e., that the spectrum decays as q^{-4}, q being the radial wave number. This translates to n^{-3} on a reference sphere (Knudsen, 1987). Under this consideration Eq. 3.15 can be written as (Knudsen, 1991):

$$\left(\sigma_n^{\zeta^c}\right) = \left(\frac{10^3}{10^3 + n^3}\right) b\left(\frac{k_2^3}{k_2^3 + n^3} - \frac{k_1^3}{k_1^3 + n^3}\right). \tag{3.16}$$

It should be noted that in recent studies, e.g., Vergos & Tziavos (2007), where a high-resolution MDT model has been used for the Mediterranean Sea (Rio & Hernandez, 2004), the corresponding cut-off frequency for the Wiener filter was found equal to ~200 km. Therefore, it is worth mentioning that its selection is empirical and it is based on maximum noise reduction with minimum signal loss taking into account the characteristics of the area under study (high/low-variability, strong/weak signal).

In Knudsen (1991) a model of the signal degree variances of the time-varying sea surface topography $\delta\zeta$ has also been introduced. According to Knudsen (1991) since $\delta\zeta$ varies with time, time-dependency should be introduced in the computation of $\boldsymbol{C}_{\delta\zeta\delta\zeta}$ in a way that temporal correlations have a behavior similar to the spatial ones. Therefore, for some time-separated points $\Delta t = |t - t'|$ the covariance function can be expressed as:

$$\mathbf{C}_{\delta\zeta\delta\zeta}\left(\psi,\Delta t\right)=\begin{Bmatrix}\sum_{n=0}^{\infty}\left(\sigma_n^{\delta\zeta}\right)P_n\left[\cos\left(\psi+\kappa^{\delta\zeta}\Delta t\right)\right] & for\ \left(\psi+\kappa^{\delta\zeta}\Delta t\right)\le\pi\\ 0 & for\ \left(\psi+\kappa^{\delta\zeta}\Delta t\right)>\pi\end{Bmatrix}. \tag{3.17}$$

In Eq. 3.17, $\kappa^{\delta\zeta}$ is a conversion factor representing in the case of the time-varying SST the correlation time of the signal. This should be studied and determined in each region under study, since the characteristics of $\delta\zeta$ vary significantly for each area and in open or closed sea regions. In Eq. 3.17 for the covariance function and the resulting covariance matrix to be positive definite the degree variances should be non-negative and their sum finite (Moritz, 1980). As far as the conversion factor is concerned Knudsen (1991) has determined it to be equal to 0.53^{o} day^{-1} for a study area in the Faeroe Islands. In complete analogy to the determination of the degree variances of the MDT presented in Eq. 3.15 the degree variance model of the time-varying SST can be described with the following formula:

$$\left(\sigma_n^{\delta\zeta}\right)=b\left(\frac{k_2^3}{k_2^3+n^3}-\frac{k_1^3}{k_1^3+n^3}\right). \tag{3.18}$$

In the same manner as for the MDT, the signal degree variances of $\delta\zeta$ are filtered by a Winer-type of filter. Therefore, taking into account that $\delta\zeta$ is just the residual signal of the complete sea surface topography after removing the contribution of ζ^c, the final analytic model of the $\delta\zeta$ degree variances can be written as:

$$\left(\sigma_n^{\delta\zeta}\right)=\left(1-\frac{10^3}{10^3+n^3}\right)b\left(\frac{k_2^3}{k_2^3+n^3}-\frac{k_1^3}{k_1^3+n^3}\right). \tag{3.19}$$

Once again, the parameters b, k_1, k_2, $\kappa^{\delta\zeta}$ are determined empirically so that the analytic model fits the empirical values describing the statistical characteristics of the time-varying sea surface topography in the area under study and more precisely the variance, the correlation length and the correlation time. Having determined all the covariance functions needed, one can apply the usual LSC solution outlined in §2 & §3 to obtain an estimation of any functional related to the Earth's gravity field through Eq. 3.12.

Of great importance are the resulting covariance and cross-covariance functions obtained by Knudsen & Tscherning (2006) for the velocities of the surface currents. Under the assumption of geostrophic flow (see Pond & Pickard, 2000) the two (latitudinal and meridian) components of the current velocities can be described in terms of the MDT as:

$$u=-\frac{g}{fR}\frac{\partial\zeta^c}{\partial\phi}, \tag{3.20}$$

$$v=\frac{g}{fR\cos\phi}\frac{\partial\zeta^c}{\partial\lambda}. \tag{3.21}$$

In Eqs. 3.20 & 3.21, f denotes the Coriolis force. Based on the aforementioned equations and the availability of a MDT covariance function, Knudsen (1991) determined analytic expressions for the geostrophic velocities auto- and cross-covariance functions, which of course depend on the azimuth a_{ij} of the side connecting i and j. The resulting formulas are:

$$\mathbf{C}_{uu}=\frac{g^2}{f_i f_j}\left(-\cos a_{ij}\cos a_{ji}\mathbf{C}_{ll}-\sin a_{ij}\sin a_{ji}\mathbf{C}_{qq}\right), \tag{3.22}$$

$$\mathbf{C}_{vv}=\frac{g^2}{f_i f_j}\left(-\sin a_{ij}\sin a_{ji}\mathbf{C}_{ll}-\cos a_{ij}\cos a_{ji}\mathbf{C}_{qq}\right), \tag{3.23}$$

$$\mathbf{C}_{u\zeta^c}=-\frac{g}{f_i}\cos a_{ij}\mathbf{C}_{l\zeta^c}, \tag{3.24}$$

$$\mathbf{C}_{v\zeta^c} = \frac{g}{f_i}\sin a_{ij}\mathbf{C}_{l\zeta^c}\,. \tag{3.25}$$

In Eqs. 3.22-3.25 the covariances $\boldsymbol{C}_{ll}$, $\boldsymbol{C}_{qq}$, and $\boldsymbol{C}_{l\zeta^c}$ are given as follows:

$$\mathbf{C}_{ll} = \frac{1}{R^2}\left(\cos\psi\mathbf{C}'_{\zeta^c\zeta^c} - \sin^2\psi\mathbf{C}''_{\zeta^c\zeta^c}\right), \tag{3.26}$$

$$\mathbf{C}_{qq} = \frac{1}{R^2}\mathbf{C}'_{\zeta^c\zeta^c} \tag{3.27}$$

and

$$\mathbf{C}_{l\zeta^c} = -\frac{1}{R}\sin\psi\mathbf{C}'_{\zeta^c\zeta^c}\,, \tag{3.28}$$

where, $\mathbf{C}'_{\zeta^c\zeta^c}$ and $\mathbf{C}''_{\zeta^c\zeta^c}$ are first and second order derivatives of the MDT auto-covariance function. Taking into account the previously presented geostrophic velocities auto- and cross-covariance functions, it is possible to use LSC in order to estimate the ocean circulation in an area under study, when observables of the type presented in Eq. 3.12 are available. What should be stressed once more though is the necessity to derive covariance expressions which will fit the local characteristics of the quasi-stationary and the time-varying part of the SST in the area under study, since regional and global estimates cannot describe the statistical characteristics of the diverse oceanic environment. Extensive work on the determination of the MDT from heterogeneous data using LSC has been also performed in the frame of the GOCINA project by the group of the Danish National Space Agency (see Knudsen 2007, Knudsen *et al*. 2006, 2007a, 2007b)

4 Combination schemes using GOCE, altimetry and gravity data

This section focuses on a review of recent results obtained from combination schemes of simulated GOCE data, land and marine gravity anomalies and satellite altimetry sea surface heights (Barzaghi *et al*. 2007, 2008). The main focus has been put in assessing the performance of heterogeneous data combination for local geoid and mean dynamic topography (MDT) determination in view of the forthcoming GOCE mission using least squares collocation. The work and results presented in this section should be viewed as a continuation of what has already been presented in sections 2 and 3.

The combination problem set-up was based on simulated GOCE data using the space-wise approach (Migliaccio et al. 2007) and available land and marine gravity anomalies and altimetric heights from the mission of ERS1 in an area in western Mediterranean Sea bounded between $35^o \le \varphi \le 47^o$ and $2^o \le \lambda \le 20^o$. As mentioned in the previous sections, least squares collocation (Moritz 1980) has been and still is one of the predominant methods for local and regional geoid and gravity field determination due to, among other things, its robustness and statistical rigorousness (Sansò & Sideris 1997).

Given available gravity observations, both at land and at sea, and altimetric geoid heights a predicted geoid undulation on land and at sea areas is estimated by the well known formula:

$$\hat{\mathbf{N}} = \mathbf{C}_{sN}^T\left(\mathbf{C}_{ss} + \mathbf{C}_{vv}\right)^{-1}\mathbf{y}\,. \tag{4.1}$$

Notice that in Eq. 4.1 it is assumed that altimetric sea surface heights are corrected for the MDT, in order to represent geoid heights, since omission of this can result in errors of some cm in the area under study (Rio and Hernadez, 2004; Vergos and Tziavos, 2007). In Eq. 4.1, $\mathbf{y}$ denotes the vector of observations Δg and N, $\mathbf{C}_{ss}$ is the covariance matrix of the input signals, $\mathbf{C}_{sN}$ is the cross-covariance matrix between the input signals and the predicted N and $\mathbf{C}_{vv}$ describes the covariance of the observation noise. In spherical approximation, the covariance and cross covariance functions to be used in eq. (4.1) can be obtained by:

$$C_{\Delta g_P,\Delta g_Q} = \frac{\mu^2}{R^4}\sum_{n=n_{\min}}^{n_{\max}}(n-1)^2\,\tilde{\sigma}_n\left(\frac{R_B^2}{r_P r_Q}\right)^{n+2}P_n(t), \tag{4.2}$$

$$C_{\Delta g_P,N_Q} = \frac{1}{\bar{\gamma}} C_{\Delta g_P,T_Q}\,, \tag{4.3}$$

$$C_{\Delta g_P,T_Q} = \frac{\mu^2}{R^3} \sum_{n=n_{\min}}^{n_{\max}} (n-1)\tilde{\sigma}_n \left(\frac{R_B}{r_P}\right)^{n+2} \left(\frac{R_B}{r_Q}\right)^{n+1} P_n(t)\,, \tag{4.4}$$

$$C_{N_P,N_Q} = \frac{1}{\bar{\gamma}^2} C_{T_P,T_Q}\,, \tag{4.5}$$

$$C_{T_P,N_Q} = \frac{1}{\bar{\gamma}} C_{T_P,T_Q}\,, \tag{4.6}$$

$$C_{T_P,T_Q} = \frac{\mu^2}{R^2} \sum_{n=n_{\min}}^{n_{\max}} \tilde{\sigma}_n \left(\frac{R_B^2}{r_P r_Q}\right)^{n+1} P_n(t)\,, \tag{4.7}$$

where $t = \cos\psi$, ψ is the spherical distance, $P_n(t)$ are Legendre polynomials of degree n, R_B is the so-called radius of the Bjerhammar sphere, r_P, r_Q are the radii of the points P and Q, μ is the gravitational constant times the earth mass (GM), $\tilde{\sigma}_n$ are some adapted signal degree variances and $\bar{\gamma}$ is the mean normal gravity used throughout the simulations. Notice that Eqs. 4.2-4.7 are completely analogous to those presented in §2, with the exception of $\tilde{\sigma}_n$ since here they result from a least squares fit of analytic covariance functions to empirical values (see details below). According to (Moritz, 1980) the prediction error covariance matrix can be computed by:

$$\mathbf{C}_e = \left(\mathbf{C}_{NN} - \mathbf{C}_{sN}^T \left(\mathbf{C}_{ss} + \mathbf{C}_{vv}\right)^{-1} \mathbf{C}_{sN}\right), \tag{4.8}$$

where, the matrix $\mathbf{C}_{NN}$ is computed from the predicted covariances of N. For comparisons with the actual errors computed from simulations, the point-wise predicted standard deviation (std) σ_i of the estimated geoid height with integer index i can be used:

$$\sigma_i = \sqrt{\mathbf{C}_e(i,i)}\,, \tag{4.9}$$

If in the combination scheme outlined in Eq. 4.1 the input vector includes data from the GOCE mission, i.e., observations of the potential T and of its second order derivatives T_{rr} in a grid at satellite level, so that

$$\mathbf{y} = \left[\mathbf{N}^T \quad \boldsymbol{\Delta}\mathbf{g}^T \quad \mathbf{T}^{\mathbf{os}T} \quad \mathbf{T}_{\mathbf{rr}}^{\mathbf{os}T}\right]^T. \tag{4.10}$$

then, complementary to Eqs. 4.2-4.7, the covariance functions of T and T_{rr} as well as their cross-covariances are also needed. These are described in accordance to Eqs. 2.9-2.14, which if the signal degree variances c_n are substituted by the adapted signal degree variances $\tilde{\sigma}_n^2$ become (Barzaghi et al. 2008):

$$C_{T_{rrP},T_{rrQ}} = \frac{\mu^2}{R^6} \sum_{n=n_{\min}}^{n_{\max}} (n+1)^2 (n+2)^2 \tilde{\sigma}_n \left(\frac{R_B^2}{r_P r_Q}\right)^{n+3} P_n(t)\,, \tag{4.11}$$

$$C_{T_{rrP},T_Q} = \frac{\mu^2}{R^4} \sum_{n=n_{\min}}^{n_{\max}} (n+1)(n+2)\ \tilde{\sigma}_n \left(\frac{R_B}{r_P}\right)^{n+3} \left(\frac{R_B}{r_Q}\right)^{n+1} P_n(t)\,, \tag{4.12}$$

$$C_{\Delta g_P,T_{rrQ}} = \frac{\mu^2}{R^5} \sum_{n=n_{\min}}^{n_{\max}} (n-1)(n+1)(n+2)\ \tilde{\sigma}_n \left(\frac{R_B}{r_P}\right)^{n+2} \left(\frac{R_B}{r_Q}\right)^{n+3} P_n(t)\,, \tag{4.13}$$

$$C_{T_{rr}P,N_Q} = \frac{1}{\bar{\gamma}} C_{T_{rr}P,T_Q} \,. \tag{4.14}$$

The notation used in Eqs. 4.11-4.14 is the same as before. It is obvious that the signal and error cross-covariance matrices used in output signal prediction Eq. 4.1 and the estimation of the error matrix will now include the covariances and cross-covariances of T and T_{rr} as well.

In the context of Barzaghi et al. (2007, 2008), which are reviewed in this section, a comprehensive analysis of the spectral content of the data and of their covariance functions has been performed. Therefore, covariance functions for all functionals used as inputs, i.e., Δg, N, T, T_{rr} have been computed. This was done by fixing first a set of degree variances to the signal degree variances from the simulated input signal used. The latter was based on the differences between EGM96 (Lemoine *et al.* 1998) and EIGEN-GL04C (Förste et *al.* 2007), which were used as the true and reference models respectively. For degrees 2 to 360 the values used are

$$\sigma_n = \sum_{m=0}^{n} \left(C_{nm}^2 + S_{nm}^2 \right), \tag{4.15}$$

where C_{nm} and S_{nm} are the coefficients of degree n and order m up to degree and order 360. For degrees 361 and above, the well-known analytical model proposed by Tscherning & Rapp (1974) was used, i.e., :

$$\sigma_\ell = \frac{a}{(\ell - 1)(\ell - 2)(\ell + 24)} \,. \tag{4.16}$$

In Eq. 4.16, a is a scale parameter, selected so that the degree variances are similar in magnitude to the degree variances obtained from the GPM98 (Wenzel 1998) up to degree 720. It should be mentioned that in the simulations, and in order to achieve a high-resolution representation of the geoid in the area, all data sources have been augmented with signal from GPM98 from degree 361 to 720 and order 0 to 720. The variance for each of the four data types has been computed (from the aforementioned covariance functions at $\psi = 0$) for different maximum degrees of summation $n_{\max}$.

From the results achieved in Barzaghi et al. (2007, 2008) it was concluded that as far as the gravity anomaly variances were concerned, the cumulative noise variance increased significantly with increasing maximum degree of summation, even at degree 1500. Even though the simulated noise was set equal to 5×10^{-5} ms^{-2} std, the cumulative signal up to degree 200 had a variance smaller than that. Therefore it was concluded that the low degree residuals could not be represented very well by gravity anomalies on a limiting area. When the potential at satellite altitude was examined, it was found that the cumulative variance after degree 100 does not change significantly. This was a clear proof of signal attenuation because of the satellite altitude, confirming that the information content of this type of data is of low resolution and regards long wavelengths only. The error std was determined at the 0.022 m^2s^{-2} level which was small with respect to the signal variance (0.14 m^2s^{-2} for degree 15), so that the low harmonic degrees are represented very accurately. A similar behaviour is seen for the second order radial derivatives T_{rr} at satellite altitude, with the difference that in this case, the variance is significant up to degree 150, and the very first harmonic degrees are not represented very well. To the available grid a simulated noise of 0.61×10^{-12} s^{-2} was assigned, so that up to degree 150 the representation of the signal is excellent. An interesting conclusion was drawn after taking a zoom around degree 200, from which it was visible that the variance still increased, so it was concluded that GGMs estimated from GOCE gradient observations can be useful up to degree 250 as it was also found in Migliaccio *et al.* (2007). From this analysis, an important conclusion was drawn, i.e., that computations with gravity anomalies aided by GOCE data give an improvement in geoid estimates (see Barzaghi *et al.* 2007) since gravity anomalies are not really sensitive to low degrees, while GOCE data can provide valuable information in this band of the gravity field spectrum, so that the two types of observations are complementary. When the geoid cumulative degree variances are examined, it is seen that it contains signal at all degrees, both low and high. So, when geoid computation is sought and at the same time we leave a direct observation of it, as it would happen with altimetry if we know a perfect model of MDT, only a filtering of the available (geoid) observations would be needed; in this sense, the four data types considered in this work would become redundant. Nevertheless, if errors exist in the available altimetric data, e.g., orbital errors, MDT omission due to unavailability of a proper model, tide misrepresentation, etc., then the information coming from GOCE observables, i.e., the potential and its second order derivatives, become strictly necessary in order to represent accurately low-frequencies and identify and remove the aforementioned errors.

Following this analysis about the covariance functions of the observations, a geoid computation was performed with least squares collocation on a 12′×12′ spherical grid and the area was split in twentyfour 3°×3°

cells, so that the coordinate limits of cell (i, j) are computed as: $\varphi_{\max} = 47 - 3(i-1)$, $\varphi_{\min} = \varphi_{\max} - 3$, $\lambda_{\min} = 2 + 3(j-1)$ & $\lambda_{\max} = \lambda_{\min} + 3$, where i=1,2,…,4 and j=1,2,…,6. Separate collocation solutions have been determined for each cell taking a 1° cell overlap for Δg and N and a 2-4° cell overlap for T and T_{rr} in order to get a more representative picture of the statistical characteristics of GOCE data. In each cell local empirical covariance functions have been determined for all four input functionals and a set of degree variances $\tilde{\sigma}_n^2$ was computed for each data type, so that the analytic covariance functions outlined in the previous section fit the empirical ones.

As mentioned at the beginning of §4 the degree variances $\tilde{\sigma}_n^2$ have been determined after a least squares (LS) fit of all four empirical covariance functions which were used as observations in the fit. In this LS adjustment scheme the design matrix for each observation covariance has as many rows as the its empirical covariance values (observations) and as many columns as the degrees used; here there are 719 columns that correspond to degrees from 2 to 720. Thus, for the potential covariance function, the design matrix is:

$$A_T(i, j) = \left(\frac{\mu}{R}\right)^2 \left(\frac{R_B}{R_B + h_{sat}}\right)^{2n+2} \sigma_n P_n(t_i), \tag{4.17}$$

where row i refers to the empirical covariance value i with spherical distance ψ_i (t_i=$cos\psi_i$) and constant height for all points of the grid h_{sat}, and column j refers to degree $n = j+1$. The unknowns of the adjustment are thus just scales for the contribution of every degree to the observed empirical covariances with respect to some prior degree variances $\tilde{\sigma}_n^2$ computed from Eq. 4.15 for degrees 2 to 720, so that we put $\sigma_n^2 = x_n \tilde{\sigma}_n^2$. In a similar way the design matrices for the other functionals are:

$$A_{\Delta g}(i, j) = \left(\frac{\mu}{R^2}\right)^2 \left(\frac{R_B}{r_{\Delta g}}\right)^{2n+4} (n-1)^2 \sigma_n P_n(t_i), \tag{4.18}$$

$$A_N(i, j) = R_B^2 \left(\frac{R_B}{r_N}\right)^{2n+2} \sigma_n P_n(t_i), \tag{4.19}$$

$$A_{T_{rr}}(i, j) = \left(\frac{\mu}{R_B^3}\right)^2 \left(\frac{R_B}{R_B + h_{sat}}\right)^{2n+6} (n+1)^2 (n+2)^2 \sigma_n P_n(t_i). \tag{4.20}$$

When the four functional matrices are used together in the adjustment, they are weighted in order to avoid numerical instabilities (e.g., T has a different magnitude from T_{rr}). A simple least squares fit though, is not convenient, for two reasons: a) too many empirical covariance values would be needed for all 719 parameters to be estimated and b) there will be negative estimated of some parameters that are not acceptable; in fact, the degree variances must be positive (Tscherning 1977). However, the estimation problem was solved by applying a regularization based on the minimization of the following hybrid norm:

$$\boldsymbol{\nu}^T \boldsymbol{\nu} + \beta \mathbf{x}^T \mathbf{K} \mathbf{x} = min, \tag{4.21}$$

where ν is the vector of residuals of the least squares fit to the empirical covariance values, $\mathbf{x}$ is the vector of parameters, β is a regularization parameter (positive scale) and $\mathbf{K}$ is a matrix making the expression $\mathbf{x}^T\mathbf{K}\mathbf{x}$ equal to the sum of the squares of the differences between two consecutive parameters. An extensive discussion on the implications of the selection of the regularization parameter β, the form of matrix $\mathbf{K}$ and the iterative character of the entire process can be found in Barzaghi et *al.* (2008).

From the covariance fit experiments performed it became evident once again that GOCE data and gravity anomalies have a complementary character. The former dominate the low degrees, while the latter dominate the high degrees, so that a good fit is achieved in every cell when T, T_{rr} and Δg are used simultaneously. An example is given for cell (4,4) in the area previously described and are presented in Figures 2-4 for the gravity anomalies, potential and second order derivatives covariance functions. Note that if only Δg empirical covariance function is used for the estimation of $\tilde{\sigma}_\ell$ then the corresponding covariance functions of T and T_{rr} do not fit well the empirical ones (Figures 3-4). On the other hand if only T and T_{rr} empirical covariance functions are used for the estimation of $\tilde{\sigma}_\ell$ then the corresponding covariance function of Δg does not fit well the empirical one (Fig. 2). It

can therefore be concluded that the addition of GOCE data to local geoid computations improves also the local degree variances estimation. In fact with Figures 3 and 4 it is shown that the lack of long wavelength information of gravity anomalies leads to a poor estimation of the low degrees $\tilde{\sigma}_\ell$ for those data only. Then, this is a new contribution of the addition of GOCE data, i.e., a better estimation of the covariance function estimation.

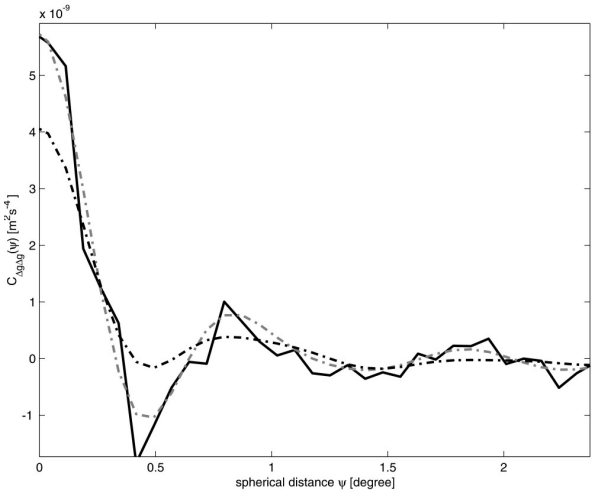

Figure 2: Gravity anomaly empirical covariance function (black solid line), analytical function corresponding to the degree variances computed from the fit to the empirical covariance functions of Δg, T_{rr} and T (grey dotted-dashed line), and analytical function corresponding to the degree variances computed from the fit to the empirical covariance functions of T_{rr} and 650 T (black dotted-dashed line) for cell 4,4.

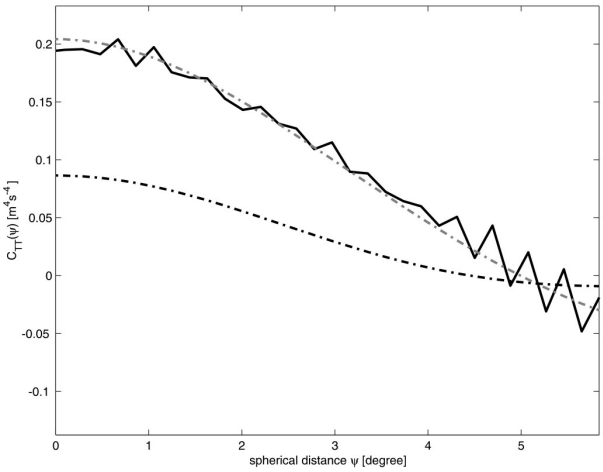

Figure 3: Potential empirical covariance function (black solid line), analytical function corresponding to the degree variances computed from the fit to the empirical covariance functions of Δg, T_{rr} and T (grey dotted-dashed line), and analytical function corresponding to the degree variances computed from the fit to the empirical covariance function of Δg (black dotted-dashed line) for cell 4,4.

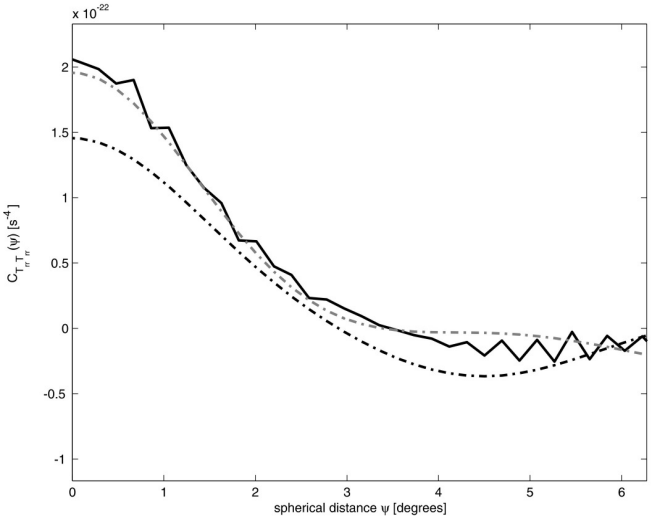

Figure 4: Radial derivatives empirical covariance function (black solid line), analytical function corresponding to the degree variances computed from the fit to the empirical covariance functions of Δg, T_{rr} and T (grey dotted-dashed line), and analytical function corresponding to the degree variances computed from the fit to the empirical covariance function of Δg (black dotted-dashed line) for cell 4,4.

With the inclusion of satellite altimetry data and their corresponding geoid empirical covariances there is redundant information. A first conclusion immediately drawn in these experiments was that the analytical functions did not fit well the altimetric empirical ones for most cells in the area under study. After a closer examination though, it became apparent that this was due to the fact that altimetry data referred to areas with a much smaller geoid variance compared to that of gravity data. A case like that can occur when altimetric data refer to areas with low geoid variability and gravity data to areas of rough terrain like the Alps. As a result of that the altimetry-derived geoid empirical covariances seemed to correspond to smaller degree variances $\tilde{\sigma}_n$ than those implied by the empirical covariance functions of the other three data types used together. A solution to that drawback comes from GOCE data, since after extending the geoid grid with a 3 or 4 degrees overlap (to match

the GOCE data area used in the region under study), the empirical geoid covariance function computed from this grid, fits the propagated analytic function coming from $\tilde{\sigma}_n$ estimated from the other three data types very well. In marine areas the geoid empirical covariance function from altimetry, the corresponding propagated geoid covariance function coming from the other three functionals and the geoid empirical function from a grid extension (a grid of geoid generated so as to cover also some land areas) are all in agreement.

From the geoid prediction results derived with all possible data combination schemes (single type solutions and all kinds of multi-type data combination) it was concluded that the addition of GOCE data to gravity anomalies Δg and satellite altimetry geoid heights N leads to significant improvement, since a marked decrease in the estimation errors was evident when more data types were incorporated in the collocation solution (Barzaghi *et al.* 2007, 2008). In addition to the reduction in the prediction error, edge effects, data gaps and distribution problems are much attenuated with the inclusion of GOCE data. In purely marine areas where good quality geodetic mission altimetry data are used, the predicted geoid error in the altimetric-only solution is very low (±1-2 cm level) (*ibid.*). When adding Δg as another input functional the solution deteriorates, while GOCE data provide only a small improvement (by a few mm) compared to the altimetric-only one. This is of course an optimistic view of altimetric marine geoid modelling, since it presumes that the MDT signal removed, is of very high-quality, so that no mean value problems remain and the propagated error in the geoid solution is small. It is well-known though, that especially in closed sea areas, the available MDT and ocean circulation models are of questionable quality, since most of them come from the altimetric data, they display a high-correlation with the altimetric geoid model errors as well as problems close to the coastline and the islands which dominate areas like the Mediterranean Sea. Moreover, in-situ oceanographic observations which could provide an independent estimation of the MDT, are few in closed sea areas contrary to the more common case of open areas like in the Atlantic and Pacific Oceans, where campaigns for large scale circulation studies and cross-calibration with altimetric satellites are conducted. But, even in areas where oceanographic observations are available, their small number and ship track-like pattern do not allow for an independent high-resolution determination of the MDT. So another experiment for geoid determination was done with the inclusion of the MDSST signal to the altimetric sea surface height observations. After repeating the geoid prediction for all cells in the area under study, it was found that the effect of the MDT is visible in marine areas only. For the same area referred to above, the error rms error increases to 12.4 cm with a std of 3.2 cm when the MDT signal is added. This is a good picture of the problems caused in altimetric marine geoid modelling when a MDT model is used to reduce the SSH data. Of course, such a free-air correction is mandatory if the geoid surface is needed as opposed to the case that the mean sea surface is determined. A good solution to this common problem in marine geoid modelling comes from GOCE data. In the aforementioned experiment, when T_{rr} and T data were added, part of the original accuracy was restored (std of 3.4 cm) and the mean value problem evident in the altimetry-only solution was removed, since the error rms droped to 3.6 cm. Higher frequency information was restored with the addition of gravity anomalies, since the error std drops to 2.9 cm when Δg, T_{rr} and T data were added.

From such results in data combination studies including GOCE data it can be concluded that: a) in all cases geoid prediction errors are improved significantly when heterogeneous data are implemented in the solution compared to single type solutions, b) it is important to obtain rigorously fitted local covariance functions that describe adequately the statistical characteristics of the data in the area, especially when the region under study has varying topography and mixed both land and marine areas (see also Barzaghi *et al.* 2007, 2008), c) long-wavelength errors coming from both gravity anomalies on land and altimetric geoid heights at sea are reduced in all cases when GOCE data enter the solution, d) the addition of GOCE data will benefit geoid modelling and gravity field approximation in general over both marine and land areas by, among other things, identifying and consequently correcting long-wavelength and other possible errors.

5 The second order kriging; a new proposal for the analysis of altimetric data

Along the same frame of employing heterogeneous data for geoid estimation, a new proposal is presented for the analysis of altimetric data using what we call second order kriging. We send to (Wackernagel 2003) for a general review of this technique. So, let us write the altimetric observation equation (2.1) in the form

$$h_t = a + bt + s_t + v_t, \quad (t = 1, 2, 3, ..., \Delta), \tag{5.1}$$

where all terms are referred to a single satellite track i, so that we do not need to use this index explicitly (as in Eq. 2.1), and can put the origin of times at D_i, because we need here to reason on the time span of the track i only. Also, in Eq. 5.1 we have denoted the combined effect of signals N_t and ζ_t in a common signal denoted by s_t, i.e. it is just

$$s_t = N_t + \zeta_t \,. \tag{5.2}$$

The concept of optimal linear estimation/prediction already introduced in §2 and further illustrated in §3 and §4, relies essentially on the possibility of knowing a priori the second order moments (covariances) of all signals that we want to predict. When these are not known, we have to estimate them from available data. As for the anomalous potential *T* we can always use the free-air gravity anomalies in the area and a covariance function of the form presented in Eq. 2.5 to infer the degree variances $c_n\left(T\right)$, especially when we adopt a parametric model, e.g., that of Tscherning and Rapp (see Tscherning and Rapp 1974).

If we had then a means to estimate the covariance of $s\left(P\right) = N\left(P\right) + \zeta\left(P\right)$ from available data, then we could know as well $C_{\zeta\zeta}\left(P,Q\right)$, because, thanks to our hypothesis of independence of *N* from ζ (see point (viii) in §2), we must have

$$C_{ss}\left(P,Q\right) = C_{NN}\left(P,Q\right) + C_{\zeta\zeta}\left(P,Q\right). \tag{5.3}$$

We propose here a new method of estimating $C_{ss}\left(P,Q\right)$ from the observations given in Eq. 5.1, which is based on a slight generalization of the kriging concept. We notice first of all that due to the hypothesis of homogeneity and isotropy of both *T* and ζ, and that of *s(P)* too, we will have

$$C_{ss}\left(P,Q\right) = C_{ss}\left(\psi_{PQ}\right). \tag{5.4}$$

Furthermore, since the orbits of the altimetric satellites are close to circular and their motion has an almost constant angular velocity, we can put along one of our tracks

$$C_{ss}\left(P_t, P_{t+\tau}\right) = C_{ss}\left(\psi_{P_t P_{t+\tau}}\right) = C_{ss}\left(\tau\right), \tag{5.5}$$

since the time difference between the two sub-sequent satellite points is $\Delta t = \tau$. What we want to find is an empirical estimator of $C_{ss}\left(\tau\right)$, namely a quadratic function of the sample data $\left\{s_t\right\}$ such that its mean value is equal to (or close to) $C_{ss}\left(\tau\right)$.

If we knew a-priori the parameters *a* and *b* in Eq. 5.1, then we could subtract $a + bt$ from the signal $y\left(t\right)$ and then compute the ordinary estimator

$$\hat{C}\left(\tau\right) = \frac{1}{\Delta - \tau}\sum_{1}^{\Delta-\tau}{}_t\left(y - a - bt\right)\left(y - a - bt - b\tau\right). \tag{5.6}$$

Since we do not know *a* and *b*, in order to use Eq. 5.6, we have first to estimate them from the available data and then use these estimates $\hat{a},\hat{b}$ instead of a, b. This approach has been criticized in the general statistical literature (see Cressie 1993 and Wackernagel 2003) and a solution has been given in terms of the so-called kriging theory. The criticism is based on that optimal $\hat{a},\hat{b}$ can be derived only if we know the covariance structure of $s_t + v_t$, otherwise the covariance of the estimation error $e\left(t\right) = \left(a - \hat{a}\right) + \left(b - \hat{b}\right)t$ can contaminate significantly the covariance presented in Eq. 5.6, since it now becomes

$$\hat{C}\left(\tau\right) = \frac{1}{\Delta - \tau}\sum_{1}^{\Delta-\tau}{}_t\left(y - \hat{a} - \hat{b}t\right)\left(y - \hat{a} - \hat{b}t - \hat{b}\tau\right). \tag{5.7}$$

Such a criticism might be less urgent when we have many data for a long time span Δ, though, even for sequences of hundreds of data the error in $\hat{a}$ and $\hat{b}$ can have a significant impact in our prediction work. In fact, as it will be shown in next paragraph, the correlated signal *s*, due to the limited number of data in the sample, can display a quite important pseudo- bias and a pseudo-tilt. So when we go to tracks confined to an internal sea, like the Mediterranean, they are necessarily short and the expected estimation error for *a* and *b* becomes even larger. Considering the shape of this area, the inclination of the orbits, the velocity of the satellites and the fact that one measurement per second is taken (actually this is a mean of 1000/s pulses for SEASAT and GEOSAT and

4000/s pulses for T/P, which generate approximately 128 waveform samples from which the instantaneous sea surface height is derived (Chelton *et al.* 2001), we can hardly find tracks in the Mediterranean Sea with more than 200 data, while 100 observations or even less is more the rule than the exception.

As we have already recalled a solution has been found by kriging theory which, instead of the covariance $C(\tau)$ uses the so-called variogram (or Kolmogorov's structure function), defined by the formula

$$\gamma(\tau) = \frac{1}{2}\mathrm{E}\left\{\left[\Delta_\tau s(t)\right]^2\right\} = \frac{1}{2}\mathrm{E}\left\{\left[s(t+\tau) - s(t)\right]^2\right\}. \tag{5.8}$$

Since $\gamma(\tau)$ is based on averaging the square of a first order difference operator, it is clear that any bias in the data is eliminated from an empirical estimator of the form

$$\hat{\gamma}(\tau) = \frac{1}{2(\Delta-\tau)}\sum_{1}^{\Delta-\tau}{}_t\left[y_{t+\tau} - y_t\right]^2 . \tag{5.9}$$

Yet, since we have a tilt parameter too in our model, namely the observation equation 5.1, we see that

$$\mathrm{E}\left\{\hat{\gamma}(\tau)\right\} = \frac{1}{2}b^2\tau^2 + \gamma(\tau) + 2\sigma_v^2, \tag{5.10}$$

i.e., $\hat{\gamma}(\tau)$ is still affected by *b*. The situation is dealt with in literature by the so-called universal kriging theory (see Wackernagel 2003). There, the variogram is substituted by a so-called generalized covariance function. However, not many recipes for its empirical estimation are given. Here we propose the use of a second order variogram which is much simpler and can be easily estimated, taking into account the repeat pattern of data points, namely *t=1,2,3,...Δ*.

We can define the second order variogram as

$$\Gamma_s(\tau) = \frac{1}{2}\mathrm{E}\left\{\left[\Delta_\tau^2 s_t\right]^2\right\} = \frac{1}{2}\mathrm{E}\left\{\left[s_{t+2\tau} - 2s_{t+\tau} + s_t\right]^2\right\}, \tag{5.11}$$

The motivation for introducing the definition in Eq. 5.11 is twofold. On one side, by taking the second difference of equation 5.1 one gets

$$\Delta_\tau^2 y_t = y_{t+2\tau} - 2y_{t+\tau} + y_t = \Delta_\tau^2\left(s_t + v_t\right), \tag{5.12}$$

because $\Delta_\tau^2 1 = 0$, $\Delta_\tau^2 t = 0$, i.e., linear functions are eliminated by the Δ_τ^2 operator. Therefore, considering that

$$\frac{1}{2}\mathrm{E}\left\{\left[\Delta_\tau^2 v_t\right]^2\right\} = \frac{1}{2}\mathrm{E}\left\{\left[v_{t+2\tau} - 2v_{t+\tau} + v_t\right]^2\right\} = 3\sigma_v^2, \tag{5.13}$$

and that $\{s_t\}$ and $\{v_t\}$ are uncorrelated sequences, we finally arrive, according to the definition of the second order variogram in Eq. 5.11, to

$$\Gamma_y(\tau) = \Gamma_s(\tau) + 3\sigma_y^2 . \tag{5.14}$$

On the other side, the definition of $\Gamma(\tau)$ opens the way to an empirical estimation through the obvious formula

$$\hat{\Gamma}_y(\tau) = \frac{1}{2(\Delta-2\tau)}\sum_{1}^{\Delta-2\tau}{}_t\left[y_{t+2\tau} - 2y_{t+\tau} + y_t\right]^2 , \tag{5.15}$$

The combination of Eqs. 5.14 and 5.15 yields an estimation procedure for $\hat{\Gamma}_s(\tau)$ and $\hat{\sigma}_v^2$. In fact $\hat{\sigma}_v^2$ can be estimated by the so-called nugget effect (see Wackernagel 2003) in Eq. 5.15, namely by taking

$$\hat{\sigma}_v^2 = \frac{1}{3}\hat{\Gamma}_y\left(0^+\right). \tag{5.16}$$

Notice that in this relation $\hat{\Gamma}_y\left(0^+\right)$ is not $\hat{\Gamma}_y\left(0\right)$, which is always zero, but represents the limit of $\hat{\Gamma}_y\left(\tau\right)$ when τ tends to zero from the right.

Subsequently we can put,

$$\hat{\Gamma}_s\left(\tau\right) = \hat{\Gamma}_y\left(\tau\right) - 3\hat{\sigma}_v^2, \left(\tau > 0\right). \tag{5.17}$$

We immediately note at this point that in principle $\hat{\Gamma}_s\left(\tau\right)$ can be estimated for all $\tau < \frac{\Delta}{2}$, yet it is not advisable to go over $\frac{\Delta}{4}$ because beyond this limit the empirical estimator presented in Eq. 5.15 will not use anymore the central values of $\left\{y_t\right\}$, with an obvious loss of significance. This means in our context that we shall have a number of $\hat{\Gamma}_s\left(\tau\right)$ varying between and 20 and 40, which however should be enough to infer the theoretical shape of $\Gamma_s\left(t\right)$. In this respect, we observe that one could study the general theoretical properties of $\Gamma\left(\tau\right)$ to find the proper class of random signals that could be treated in this way. Yet, this is out of the scope of this paper, where we assume that the sequence $\left\{s_t\right\}$ has a stationary covariance. In fact our aim is just to find a reliable estimator $\hat{C}\left(\tau\right)$, so that the algorithm of collocation with parameters could be applied. So the only thing we need is to develop the square in Eq. 5.11 to find

$$\Gamma_s\left(\tau\right) = 3C\left(0\right) - 4C\left(\tau\right) + C\left(2\tau\right). \tag{5.18}$$

An analogous reasoning for $\left\{y_t\right\}$ Eq. 5.15 and the observation equation 5.1 gives

$$\Gamma_y\left(\tau\right) = 3\left(C\left(0\right) + \sigma_v^2\right) - 4C\left(\tau\right) + C\left(2\tau\right). \tag{5.19}$$

If we put $\hat{\Gamma}_y\left(\tau\right)$ and $\hat{\sigma}_v^2$ in Eq. 5.19 we can use this formula as a difference equation to estimate $\hat{C}\left(\tau\right)$.

Notice that in this way the use of Eq. 5.19 depends on the knowledge of *C(0)* too and of the values *C(2τ)* for large *τ*. On the other hand if we assume, as we do, that $C\left(\tau\right) \to 0$ for $\tau \to \infty$, we can reasonably take $\hat{C}\left(\tau\right) = 0$ for $\tau > \overline{\tau}$, so that one can define all the $\hat{C}\left(\tau\right)$ values for $\tau \le \overline{\tau}$. The procedure will be illustrated in the next section by two examples, one with simulated observations and another employing sea surface height data from the exact repeat mission of TOPEX/Poseidon. It seems interesting too to note that Eq. 5.19 can be expressed in terms of the ordinary variogram. In fact, revealing that $\gamma_y\left(\tau\right) = \sigma_v^2 + C\left(0\right) - C\left(\tau\right) = \sigma_v^2 + \gamma\left(\tau\right)$, it is easy to verify that Eq. 5.19 translates into

$$\Gamma_y\left(\tau\right) = 4\gamma\left(\tau\right) - \gamma\left(2\tau\right), \tag{5.20}$$

which could also be used to derive an empirical estimator of *γ(τ)*. In fact, assuming that beyond a value $\overline{\tau}$, $\gamma\left(\tau\right)$ becomes constant, then Eq. 5.20 tells us that $\Gamma_y\left(\tau\right) = 3\gamma\left(\tau\right), \forall\, \tau > \overline{\tau}$. Then we can enter into the interval $\tau < \overline{\tau}$ and inserting from $\hat{\gamma}\left(2\tau\right) = \Gamma\left(\overline{\tau}\right)$ for $2\tau > \overline{\tau}$ we can finally get

$$\hat{\gamma}\left(\tau\right) = \frac{1}{4}\left[\Gamma\left(\tau\right) + \hat{\gamma}\left(2\tau\right)\right], \tag{5.21}$$

for $\tau = \overline{\tau} - 1, \overline{\tau} - 2, \overline{\tau} - 3, \ldots$.

6 Numerical examples

In this section we want to demonstrate the feasibility of the proposal presented in §5. For this purpose we first present two simulation examples which are treated according to slightly different approaches and which allow to assess the signal prediction error along the previous lines. In the first case the simulated track carries 400 data, in the second case only 100 data, therefore it gets closer to the short altimetric tracks found throughout the Mediterranean Sea. In both cases the numerical procedure followed has been the same, changing only the dimension of the sample.

The simulated model follows Eq. 5.1 and in particular we had adopted the following:

Linear trend: a=0.200; b=0.001; t=1, 2, 3, …, Δ; Δ=400 or Δ=100.

Signal: realization of length Δ from the stationary covariance $C(\tau) = C_o e^{-\frac{\tau}{T}}$; $\tau = 0,1,2,...,\Delta$; C_o=0.0200; T=25.

Noise: Gaussian with zero average and σ_v=0.03.

Numbers are expressed in meters for the observations and seconds for times. So the trend goes from 20 cm up to 60 cm when Δ=400 and up to 30 cm when *Δ*=100; the signal has a standard deviation value of 14 cm and the noise of 3 cm.

Note that the mean correlation time *T* is quite long; we have chosen such a high value on purpose because this produces almost deterministic waves in the data and a possible sensible linear pseudo-trend, though the theoretical average of s_t is zero. This is particularly evident in the sample of 400 data, where a pseudo-bias of 15 cm (at epoch *t=0*) and a pseudo-tilt of -0.06 cms^{-1} are present (see Figure 5). Indeed this is not always like that, for instance such an effect is much less pronounced for the sample of 100 data (see Figure 6). Yet it happens many times, according to our simulations, so we wanted to consider such an effect in one of the presented cases.

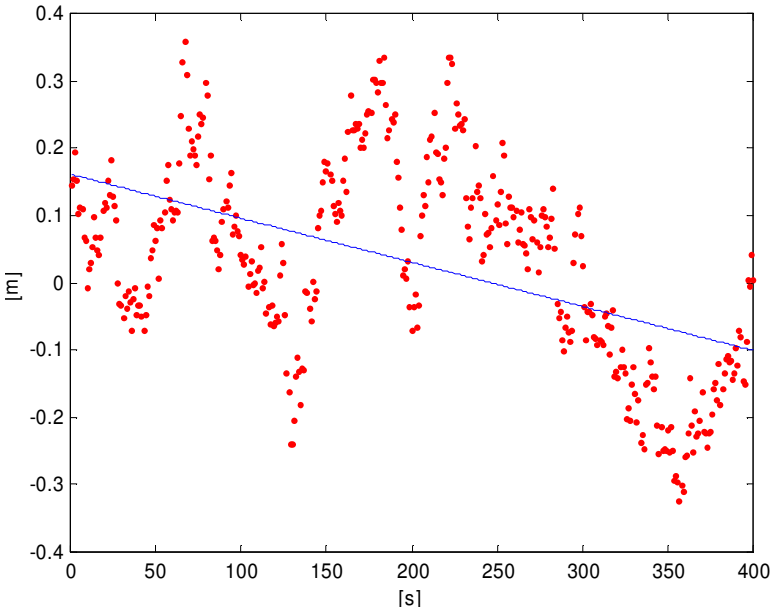

Figure 5: Simulated signal (400 values) in dotted line, pseudo-linear trend in continuous line.

Now we come to the analyses performed. For each of the two samples four results have been derived that we shall call *cov1*, *cov2*, *var1*, *var2* specifically:

cov1: bias and tilt are estimated by least squares, with a covariance matrix proportional to the identity; from the residuals an empirical covariance is estimated making it possible to calculate $\hat{C}_o$, $\hat{T}$, $\hat{\sigma}_y^2$; this is done by first identifying the model and then fitting empirical values by a simple, i.e., un-weighted least squares; finally from the residuals and the empirical covariance function a prediction of the signal, $\hat{s}_t$, is performed and the mean square prediction error is estimated from

$$\mathrm{E}=\left\{\frac{1}{\Delta}\sum_{1}^{\Delta}{}_{t}\left(\hat{s}_t-s_t\right)^2\right\}^{1/2}, \tag{5.22}$$

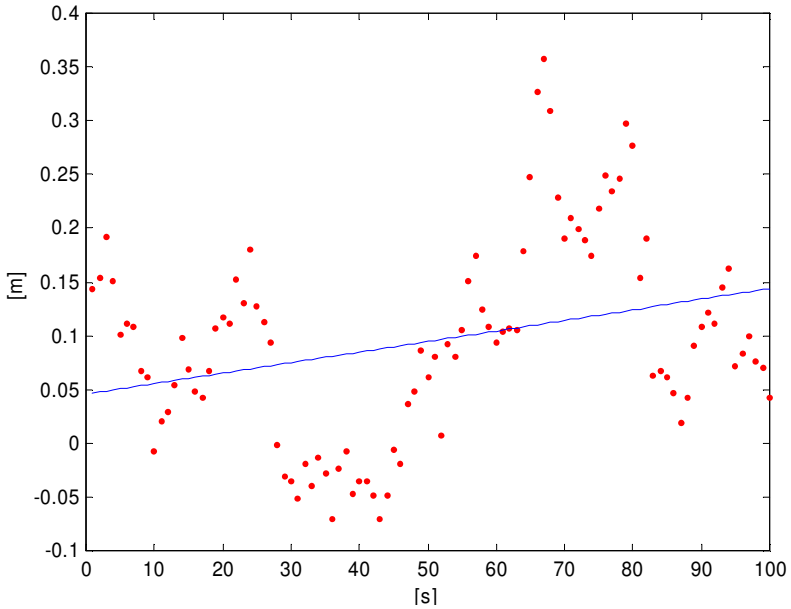

Figure 6: Simulated signal (100 values) in dotted line, pseudo-linear trend in continuous line.

cov2: is an attempt of refining *cov1* in the sense that the covariance estimated in *cov1* is now used to produce a, hopefully, better bias an tilt and then the whole estimation procedure is repeated.

var1: in this case, the second order empirical variogram $\hat{\Gamma}(\tau)$ is estimated from Eq. 5.15,

$$\hat{\Gamma}_y(\tau)=\frac{1}{2(\Delta-2\tau)}\sum_{1}^{\Delta-2\tau}{}_{t}\left[y_{t+2\tau}-2y_{t+\tau}+y_t\right]^2, \tag{5.23}$$

then an empirical covariance function $\hat{C}(\tau)$ is estimated by substituting Eq. 5.19 in Eq. 6.2, namely

$$\hat{C}(\tau)=\frac{3}{4}\left(C(0)+\sigma_v^2\right)+\frac{1}{4}C(2\tau)-\frac{1}{4}\hat{\Gamma}(\tau). \tag{5.24}$$

Eq. 5.24 is initialised by considering $\hat{C}(2\tau)=0$ above a threshold $\bar{\tau}$ and by using an estimate of $C(0)+\sigma_v^2$ as the mean quadratic value of the residuals of a simple linear regression as in *cov1*; from the empirical covariance function we then derive a positive definite model by interpolating the empirical values with a parametric family and estimating the parameters via a simple least squares;

var2: in this case we use Eq. 5.19 with the empirical estimates $\hat{\Gamma}(\tau)$, as an observation equation for some theoretical covariance family, $C_o G(\tau,\theta)$, and estimate the parameters C_o, θ by simple least squares; in order to clarify the above, in our case we put

$$\hat{\Gamma}(\tau)=A-C_o\left[4e^{-\frac{\tau}{\mathrm{T}}}-e^{-\frac{2\tau}{\mathrm{T}}}\right]+y_\tau, \tag{5.25}$$

and we linearize and solve for the parameters A, C_o, T considering that the estimated quantities have to fulfil the constrain

$$\frac{1}{3}\hat{A} - \hat{C}_o > 0\,, \tag{5.26}$$

because we can then put

$$\hat{\sigma}_v^2 = \frac{1}{3}A - \hat{C}_o\,. \tag{5.27}$$

The results of our small simulation examples are summarized in the Tables 1 and 2 listed below.

Table 1. Results of interpolation and filtering for the sample with Δ=400 (first line presents theoretical values; units in parentheses).

	a (m)	b (ms^{-1})	σ_v^2 (m^2)	C_o (m^2)	T (s)	E (m)
theoretical	0.2000	0.0010	0.0009	0.0200	25.0000	----------
cov1	0.3633	0.0003	0.0012	0.0176	24.6175	0.4770
cov2	0.3524	0.0004	0.0000	0.0175	17.4829	0.0734
var1	0.3521	0.0004	0.0012	0.0175	25.6800	0.0706
var2	0.3517	0.0004	0.0015	0.0183	27.6033	0.0706

Table 2. Results of interpolation and filtering for the sample with Δ=100 (first line presents theoretical values; units in parentheses).

	a (m)	b (ms^{-1})	σ_v^2 (m^2)	C_o (m^2)	T (s)	E (m)
theoretical	0.2000	0.0010	0.0009	0.0200	25.0000	----------
cov1	0.2532	0.0019	0.0001	0.0123	9.6834	0.0377
cov2	0.2846	0.0014	0.0000	0.0109	2.0531	0.0301
var1	0.2855	0.0013	0.0005	0.0119	10.1516	0.0277
var2	0.2953	0.0012	0.0017	0.0205	14.5654	0.0217

These two examples are typical, as for the results, of a number of trials performed and allow us to draw some conclusions:

(i) The poor performance, for all methods, in estimating the trend $a+bt$ is due to the presence of pseudo-biases and pseudo-tilts in the sampled signals as it can be seen in Fig. 5, for Δ=400, and Fig. 6, for Δ=100; in particular the phenomenon is quite relevant for the case of Δ=400 (Fig. 5) and this is also the reason why the value of E in this case is quite large.

(ii) The second step of collocation (*cov2*) does not always lead to an improvement over *cov1*.

(iii) The filtering through a step of estimation of the second order variogram is generally better that the first two methods.

(iv) The direct estimation of the covariance structure from $\hat{\Gamma}(\tau)$, i.e., (*var2*) gives generally the best results in terms of signal prediction.

Notice that the first comment in the above list justifies for a further important remark: the correct formulas for the estimation of the prediction error of the signal is the one derived from collocation theory with parameters (recalled in §2) and not the one coming from the application of standard formulas of collocation without parameters, because in the last case the influence of the estimation error of the parameters is not accounted for. In the present context it means that the covariance matrix of the error of the predicted signals $\hat{s}$ is:

$$\mathbf{C}_{ee} = \mathbf{C}_{\hat{s}\hat{s}} - \mathbf{C}_{\hat{s}s}\left[\mathbf{C}_{yy}^{-1} - \mathbf{C}_{yy}^{-1}\mathbf{A}\mathbf{N}^{-1}\mathbf{A}^T\mathbf{C}_{yy}^{-1}\right]\mathbf{C}_{s\hat{s}}\,, \tag{5.28}$$

where $\mathbf{C}_{yy} = \mathbf{C}_{ss} + \mathbf{C}_{vv}$ and $\boldsymbol{A}$ is the design matrix of the linear regression. As we see, Eq. 6.7 has an additional term with respect to the simple formula $\mathbf{C}_{ee} = \mathbf{C}_{\hat{s}\hat{s}} - \mathbf{C}_{\hat{s}s}\mathbf{C}_{yy}^{-1}\mathbf{C}_{s\hat{s}}$, and it is precisely this term that describes the influence of the error in the regression parameters.

Finally, we have analyzed as an example a true track (track no. 9 in Fig. 7) from the TOPEX/Poseidon mission in the Mediterranean Sea, which bears 131 observations of the sea surface height (see Fig. 8). The data have been first compared with a geoid profile derived from the GPM98 (Wenzel 1999) geopotential model,

tailored to the European-Mediterranean area, in order to leave into signal s_t only a small residual geoid, plus trend and SST. Then the trend (i.e., *a* and *b*) and the covariance have been estimated once with the *cov1* approach and a second time with the *var2* approach. After a first glance to the empirical covariance, we have decided to use the same exponential model as in the two simulation examples. The results are presented in Table 3, where similar symbols as in Tables 1 and 2 have been used.

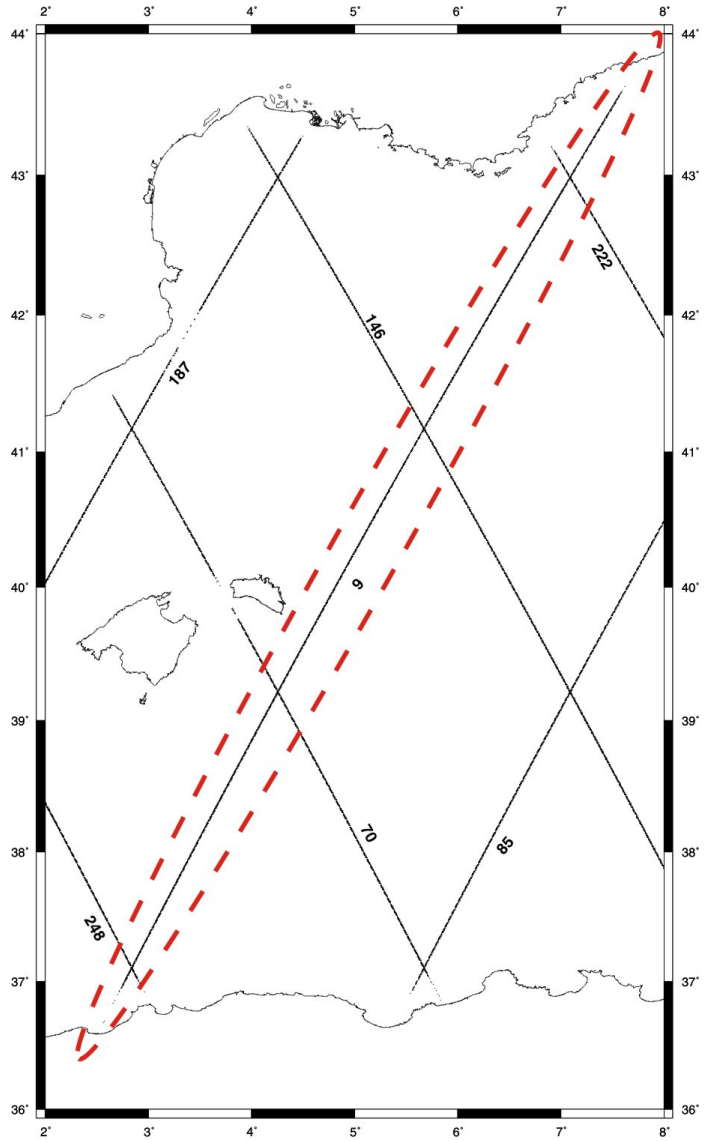

Figure 7: TOPEX/Poseidon tracks in the western part of the Mediterranean Sea (red circle denotes track no.9).

Table 3. Trend and covariance of the sea surface topography for a T/P track.

	a (m)	b (ms^{-1})	σ_v^2 (m^2)	C_o (m^2)	T (s)
cov1	0.3607	-0.0071	0.0068	0.1202	15.578285
var2	0.5802	-0.0106	0.0015	0.0612	16.045754

Naturally in this case we cannot say what is the truth and therefore we cannot decide which solution is better. Yet, we see first of all that the two estimates of *(a,b)* are significantly different; moreover, the model *cov1* with its 34 cm of signal and 8 cm of noise seems to be slightly less realistic than *var2*, with 24 cm of signal and 4 cm of noise. This agrees as well with the conclusions drawn from the simulation examples. In addition, a collocation solution along the track, performed with the sole target of filtering the noise, gives in the two cases the results shown in Fig. 9. As one can see, while the solution *cov1* has still a significant systematic error left in the residuals, the solution *var2* can follow very well the relevant features of the signal s_t.

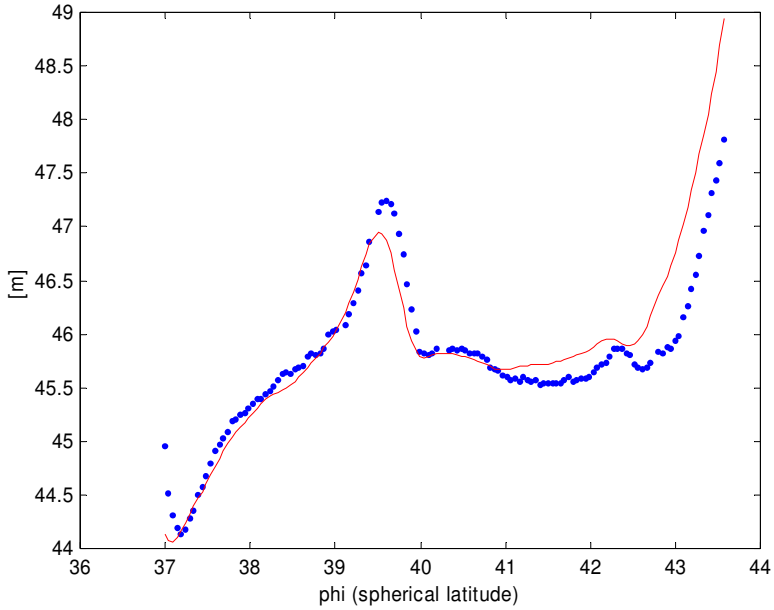

Figure 8: TOPEX/Poseidon track no. 9 sea surface heights (dotted line) and GPM98 geoid heights (solid line).

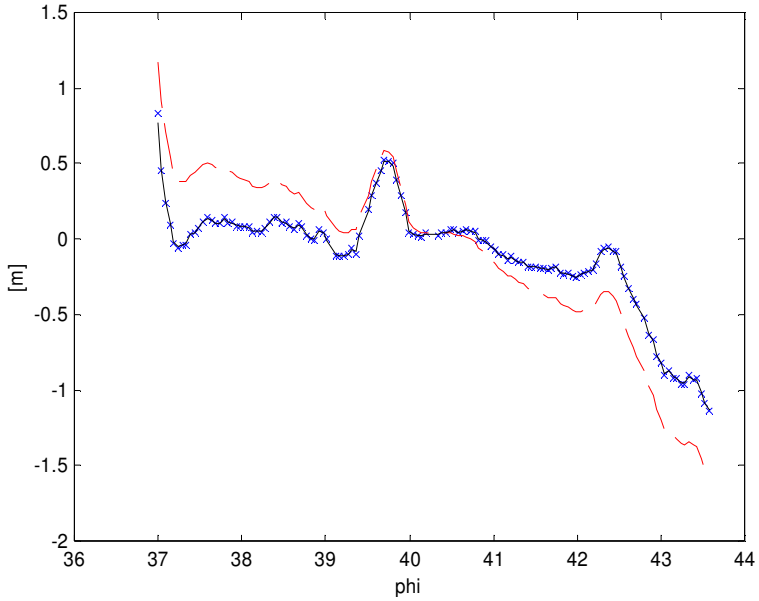

Figure 9: Observed signal (crosses), *cov1* filtered signal (dashed line), *var2* filtered signal (solid line).

7 Conclusions

A detailed review of the principles, observation and estimation equations of least-squares collocation have been presented in heterogeneous data combination schemes. An analytic description of all auto- and cross-covariance functions has been given for the combination of gravity anomalies, altimetric geoid heights, and GOCE observations of the potential and of its second order derivatives. Moreover, the spectral domain FFT-based method of Multiple Input Multiple Output System Theory has been presented with a detailed example for the combination of the aforementioned functionals of the Earth's gravity field towards the determination of geoid heights. Apart from the covariances of the input data described analytic models for the determination of the covariances of the quasi-stationary and time-varying sea surface topography have been reviewed. The main goal was to present a comprehensive and complete, from all points of view, picture of the application of LSC in the study of the Earth's gravity field and the advantage of using geodetic data and methods in the determination of oceanographic quantities like the geostrophic velocities. This is of special importance in view of the forthcoming launch of the GOCE mission in 2008.

From the results presented in the combination tests with simulated GOCE data, some important conclusions can be drawn: a) the first one is that in all cases the geoid prediction is drastically improved when all the heterogeneous data are implemented in the solution. It has been that heterogeneous data give much better

solutions than single-data type; b) what is also of utmost importance is the fact that well fitted local covariance functions need to be determined to describe the local statistical characteristics. Even in neighbouring cells in the test area, with different characteristics and mixture of land and sea, the statistical properties of the gravity field varied significantly; c) long-wavelength errors coming from both gravity anomalies on land and altimetric geoid heights at sea are reduced in all cases when GOCE data are used in a LSC solution. This is a very important fact, since it allows to separate the geoid and the MDT signal in marine areas and to remove orbital errors from altimetric SSHs. The geoid and MDT signals dominate an overlapping band of the gravity field spectrum so filtering and stacking of SSH data cannot separate them. Moreover, orbital errors in altimetric observations, which have a long wavelength signature, cannot be completely removed with crossover adjustment. Therefore, the addition of GOCE data will improve geoid modelling and gravity field approximation in general over both marine and land areas by identifying and consequently correcting long-wavelength errors; d) computations from gravity anomalies aided by GOCE data give an improvement in geoid estimates, since gravity anomalies are not really sensitive to low degrees, while GOCE data provide valuable information in this band of the gravity field spectrum. From the geoid cumulative degree variances, it is evident that they contained signal at low as well as at high degrees. So, when dealing with altimetric data, that , after a pre-processing still contain orbital errors, MDT inaccuracies, tidal errors etc, the information coming from GOCE observables is of great importance to identify and remove the aforementioned effects.

Finally, from the newly proposed application of second order kriging and the results of the simulation performed, some further important conclusions can be drawn: a) the poor performance of all methods, in estimating the trend $a+bt$ in short arcs is due to the presence of pseudo-biases and pseudo-tilts in the sampled signals as it can was seen from Figures 5 and 6. This leads to the conclusion that the correct formulas for the estimation of the prediction error of the signal are those derived from collocation theory with parameters instead of those coming from the application of standard formulas of collocation without parameters, because in the last case the influence of the estimation error of the parameters is not accounted for; b) the second step of collocation (*cov2*) does not always lead to a sensible improvement over *cov1*; c) filtering through a step of estimation of the second order variogram is generally better that applying the first two methods; d) the direct estimation of the covariance structure from $\hat{\Gamma}(\tau)$ (*var2*) gives generally the best results in terms of signal prediction. In the tests with the real T/P SSHs in the Mediterranean Sea, two solutions have been determined, i.e., one with the *cov1* and another with the *var2* model. The results with *var2*, with 24 cm of signal and 4 cm of noise can be regarded as more realistic compared to the model *cov1* with its 34 cm of signal and 8 cm of noise for the MDT. Finally, the *cov1* collocation solution along a real T/P track, performed with the sole target of filtering the noise, presents a significant systematic error in the residuals, while the solution with *var2* follows very well the relevant features of the stationary sea surface topography. Here lies the future direction of this work, which will be the comparison of the estimated ζ^c and $\delta\zeta$ both from LSC using the covariances and cross-covariances presented in §3 and the newly proposed second-order kriging approach.

ACKNOWLEDGEMENT

This work was performed under ESA contract No. 18308/04/NL/NM (GOCE HPF) and in the frame of the 3rd Community Support Program (Opp. Supp. Progr. 2000 - 2006), Measure 4.3, Action 4.3.6, Sub-Action 4.3.6.1 (International Scientific and Technological Co-operation), bilateral cooperation between Greece and Italy. The authors wish to acknowledge the constructive suggestions and comments by D.N. Arabelos and C.C. Tscherning, which led to an improved version of the paper.

REFERENCES

Andritsanos, V.D., 2000. Optimum combination of terrestrial and satellite data with the use of spectral techniques for applications in geodesy and oceanography. *PhD dissertation, Aristotle University of Thessaloniki, Department of Geodesy and Surveying*, 2000.

Andritsanos, V.D., Sideris M,G. & Tziavos, I.N., 2001. Quasi-stationery Sea Surface topography estimation by the multiple Input-Output method, *J. of Geodesy.*, **75**: 216-226.

Andritsanos, V.D. & Tziavos, I.N., 2002. Estimation of gravity field parameters by a multiple input/output system, *Phys and Chem of the Eart*h, Part A **25**(1): 39-46.

Arabelos, D.N., Forsberg, R. & Tscherning, C.C., 2007. On the a priori estimation of collocation error covariance functions: a feasibility study. *Geophys. J. Int.*, **170**(2), 527-533. doi:10.1111/j.1365-246X.2007.03460.x

Barzaghi, R., Maggi, A., Tselfes, N., Tsoulis, D., Tziavos, I.N. & Vergos G.S., 2007. Combination of gravimetry, altimetry and GOCE data for geoid determination in the mediterranean: Evaluation by simulation, acccepted to *Proc. of the IUGG XXIV General Assembly*, 02-13 July 2007, Perugia, Italy.

Barzaghi, R., Tselfes, N., Tziavos, I.N. & Vergos G.S., 2008. Geoid and high resolution sea surface topography modelling in the Mediterranean from gravimetry, altimetry and GOCE data: Evaluation by Simulation, submitted to J of Geod.

Cazenave, A., Bonnefondb, P., Merciera, F., Dominha, K. & Toumazou, V., 2002. Sea level variations in the Mediterranean Sea and Black Sea from satellite altimetry and tide gauges, *Global Plan. Change*, **34**(1-2), 59-86.

Chelton, D.B., Ries, J.C., Haines, B.J., Fu, L.-L. & Callahan, P.S., 2001. Satellite altimetry, in: *Satellite Altimetry and Earth Sciences: A Handbook of Techniques and Applications*, International Geophysics Series, **69**, pp. 4-131, eds Fu, L.-L. & Cazenave, A., Academic Press, San Diego.

Cressie, N., 1993. *Statistics for Spatial Data*, John Willey, New York.

Eeg, J. & Krarup, T., 1975. Integrated Geodesy: Methoden und Verfahren der math, Physik, Band **13**, 77-124.

Engelis, T., 1987. Spherical harmonics expansion of the Levitus Sea Surface Topography, *Reports of the Department of Geodetic Science*, **385**, The Ohio State University, Columbus, Ohio.

Fenoglio, M.L., 2002. Long term sea level change in the Mediterranean Sea from multi-satellite altimetry and tide gauges, *Phys. Chem. Earth*, **27**, 1419-1431.

Forsberg, R., Skourup, H., Andersen, O.B., Knudsen, P., Laxon, S.W., Ridout, A., Johannesen, J., Siegismund, F., Drange, H., Tscherning, C.C., Arabelos, D., Braun, A. & Renganathan, V., 2007. *Combination of Spaceborne, Airborne and In-Situ Gravity Measurements in Support of Arctic Sea Ice Thickness Mapping*, Danish National Space Institute Technical Report Series, 7, DNSC Copenhagen,

Förste, Ch., Flechtner., F., Schmidt, R., König, R., Meyer, U., Stubenvoll, R., Rothacher, M., Barthelmes, F., Neumayer, H., Biancale, R., Bruinsma, S., Lemoine, J.M. & Loyer, S., 2007. Global mean gravity field models from combination of satellite mission and altimetry/gravimetry surface data, in *Proc. of the 3rd international GOCE user workshop*, 6-8 November 2006, Frascati, Italy.

Hwang, C., Guo J.,Deng, X., Hsu, H.Y. & Liu, Y., 2006. Coastal gravity anomaly from retracked Geosat/GM altimetry: improvement, limitation and the role of airborne gravity data, *J. Geodesy*, **80**(4), 204-216, doi: 10.1007/s00190-062-0052-x.

Heiskanen, W.A. & Moritz, H., 1967. *Physical Geodesy*, W.H. Freeman, San Francisco.

Kingdon, R., Hwang, C., Hsiao, Y.-S. & Santos, M., 2008. Gravity Anomalies from Retracked ERS and Geosat Altimetry over the Great Lakes: Accuracy Assessment and Problems, *Terr. Atmos. Ocean. Sci.* **19**(1-2): 93-101.

Knudsen, P., 1987. Estimation and modelling of the local empirical covariance function using gravity and satellite altimeter data, *Bull. Geod.*, **61**, 145-160.

Knudsen, P., 1991. Simultaneous estimation of the gravity field and sea surface topography from satellite altimeter data by least-squares collocation, *Geophys. J. Inter.*, **104**(2), 307-317.

Knudsen, P., 1992. Estimation of sea surface topography in the Norwegian sea using gravimetry and Geosat altimetry, *Bull. Géod.,* **66**, 27-40.

Knudsen, P., 1993. Integration of gravity and altimeter data by optimal estimation techniques, in: *Satellite Altimetry for Geodesy and Oceanography*, Lecture Notes in Earth Sciences, **50**, 453-466, eds Rummel, R. & Sansò, F., Springer-Verlag, Berlin Heidelberg.

Knudsen, P., 2007. Integration of Altimetry and GOCE Geoid For Ocean Modeling: Results From The GOCINA Project, *in Proceedings of the 3rd International GOCE User Workshop*, ESA SP 627, 35-42, ed Fletcher, K., ESA Publications Division, ESTEC Noordwijk The Netherlands.

Knudsen, P., Andersen, O.B. & Andersson, T.B., 2007a. Optimal filtering of mean dynamic topography models, *in Proceedings of the 3rd International GOCE User Workshop*, ESA SP 627, 277-284, ed Fletcher, K., ESA Publications Division, ESTEC Noordwijk The Netherlands.

Knudsen, P., Andersen, O.B., Haines, K., Hipkins, M., Rio, H. & Johannesen, J., 2007b. Integration of Altimetry and GOCE Geoid for Ocean Modeling: Results from the GOCINA Project, in *Proceedings of the Envisat Symposium 2007*, ESA SP-636, eds Lacoste H. & Ouwehand, L., ESA Publications Division, ESTEC, Noordwijk, The Netherlands.

Knudsen, P., Andersen, O.B., Forsberg, R., Föh, H.P., Olesen, A.V., Vest, A.L., Solheim, D., Omang, O.D., Hipkin, R., Hunegnaw, A., Haines, K., Bingham, R., Drecourt, J.P., Johannessen, J.A., Drange, H., Siegismund, F., Hernandez, F., Larnicol, G., Rio, M.H. & Schaeffer, P. (2006) *GOCINA – Geoid and Ocean Circulation in the North Atlantic*, Danish National Space Institute Technical Report Series, 5, DNSC Copenhagen,

Knudsen, P. & Tscherning, C.C., 2006. Error Characteristics of dynamic topography models derived from altimetry and GOCE Gravimetry, in *International Association of Geodesy Symposia, 'Dynamic Planet 2005 - Monitoring and Understanding a Dynamic Planet with Geodetic and Oceanographic Tools'*, **130**, 11-16, eds Tregoning, P. & Rizos C., Springer-Verlag, Berlin Heidelberg.

Larnicol, G., Le Traon, P.Y. & De Mey, P., 1995, Sea level variability in the Mediterranean Sea from two years of T/P data, *J. Geophys. Res.*, **100**(C4), 25163-25177.

Le Traon, P.Y. & Ogor, F. (1998) ERS-1/2 orbit improvement using Topex/Poséidon: The 2 cm challenge, *J Geophys Res*, (**103**)C4, pp. 8045-8057.

Le Traon, P.Y., Gaspar, P., Bouyssel, F. & Makhmara, H., 1995. Using TOPEX/POSEIDON data to enhance ERS-1 orbit, *J Atm Ocean Tech*, **12**, pp. 161-170.

Lemoine, F.G., Kenyon, S.C., Factor, J.K., Trimmer, R.G., Pavlis, N.K., Chinn, D.S., Cox, C.M., Klosko, S.M., Luthcke, S.B., Torrence, M.H., Wang, Y.M., Williamson, R.G., Pavlis, E.C., Rapp, R.H. & Olson T.R., 1998. The development of the joint NASA GSFC and NIMA geopotential model EGM96, *NASA/TP-1998-206861*, Goddard Space Flight Center, Greenbelt, Maryland.

Madsen, K.S., Høyer, J.L., and Tscherning, C.C., 2007. Near-coastal satellite altimetry: Sea surface height variability in the North Sea – Baltic Sea area, *Geophys. Res. Let.*, **34**, L14601, doi:10.1029/2007GL029965.

Migliaccio, F., Reguzzoni, M. & Sansò, F., 2004. Space-wise approach to satellite gravity field determination in the presence of coloured noise, *J. of Geod.*, **78**, 304-313.

Migliaccio, F., Reguzzoni, M. & Tselfes, N., 2006. GOCE: a full-gradient Solution in the Space-wise Approach. in *International Association of Geodesy Symposia, 'Dynamic Planet 2005 - Monitoring and Understanding a Dynamic Planet with Geodetic and Oceanographic Tools'*, vol. 130, pp. 383-390, eds Tregoning, P. & Rizos C., Springer-Verlag, Berlin Heidelberg.

Migliaccio, F., Reguzzoni, M., Sansò, F., Tselfes, N., Tscherning, C.C. & Veicherts, M., 2007. The latest of the space-wise approach for GOCE data analysis, in *Proc. of the 3rd international GOCE user workshop*, 6-8 November 2006, Frascati, Italy.

Migliaccio, F., Reguzzoni, M., Sansò, F. & Tselfes, N., (submitted). An error model for the GOCE space-wise solution by Monte Carlo methods. Submitted to *Proc. of the IUGG XXIV general assembly*, 02-13 July 2007, Perugia, Italy.

Moritz, H., 1980. *Advanced Physical Geodesy*, Wichmann, Karlsruhe.

Pail, R., 2003. GOCE Data Archiving and Processing Center (DAPC) Graz, *Graz University of Technology*, Austrian Space Agency.

Pavlis, N.K., Holmes, S.A., Kenyon, S.C. & Factor, J.K., 2008. An Earth gravitational model to degree 2160: EGM2008, Presented at the *2008 General Assembly of the European Geosciences Union*, Vienna, Austria, April 13-18, 2008.

Pond, S. & Pickard, G., 2000. *Introductory dynamical oceanography*, 2nd edition, Butterworth – Heinemann.

Reguzzoni, M., Sansó, F., and Venuti, G., 2005. The theory of general kriging, with applications to the determination of a local geoid, *Geophys. J. Int.*, **162(4)**, 303-314, doi: 10.1111/j.1365-246X.2005.02662.x.

Rio, M.-H. & Hernandez F., 2004. A mean dynamic topography computed over the world ocean from altimetry, in-situ measurements and a geoid model, *J. of Geoph. Res.*, **109**(12), C12032, doi: 10.1029/2003JC002226.

Rummel, R., Gruber, T. & Koop, R., 2004. High level processing facility for GOCE: Products and processing strategy, in *Proc. of 2nd International GOCE User Workshop*. Frascati, Italy, March 8-10 2004.

Sansò, F., 1986. Statistical methods in physical geodesy, in: *Mathematical and numerical techniques in physical Geodesy*, Lecture Notes in Earth Sciences, **7**, 3-47, ed Sünkel, H., Springer-Verlag, Berlin Heidelberg.

Sansò, F. & Sideris M.G., 1997. On the similarities and differences between systems theory and least-squares collocation in physical geodesy, *Boll. di Geod. e Scie. Aff.*, **2**, 174-206.

Schrama, E.J.O., 1989. The role of orbit errors in processing of satellite altimeter data, *Netherlands Geodetic Commision. Publications on geodesy, New series*, **33**, Delft.

Sideris, M.G., 1996. On the use of heterogeneous noisy data in spectral gravity field modeling methods, *J. of Geod.*, **70**: 470-479.

Sünkel, H., 2002. From Eötvös to mGal+, in: Final Report, ESA/ESTEC contract No. 14287/00/NL/DC, GOCE Study Report, ed. Sünkel H.

Tscherning, C.C. & Rapp, R.H., 1974. Closed covariance expressions for gravity anomalies, geoid undulations, and deflections of the vertical implied by anomaly degree-variance models, *Reports of the Department of Geodetic Science*, **208**, The Ohio State University, Columbus, Ohio.

Tscherning, C.C., 1977. A note on the choice of norm when using collocation for the computation of approximation to the anomalous potential, *Bull. Geod.*, **5**1, 137-147.

Tscherning, C.C., 1986. Functional methods for gravity field approximation, in: *Mathematical and numerical techniques in physical Geodesy*, Lecture Notes in Earth Sciences, **7**, pp. 3-47, ed Sünkel, H., Springer-Verlag, Berlin Heidelberg.

Tscherning, C.C., 1993. Computation of Covariances of Derivatives of the Anomalous Gravity Potential in a Rotated Reference Frame, *Manuscr. Geod.*, **18**, 115-123.

Tziavos, I.N., Sideris, M.G. & Forsberg, R., 1998a. Combined satellite altimetry and shipborne gravimetry data processing, *Mar. Geod.*, **21**, 299-317.

Tziavos, I.N., Forsberg, R. & Sideris, M.G., 1998b. Marine gravity field modeling using shipborne and geodetic missions altimetry data, *Geomatics Res Australasia*, **69**, 1-18.

Tziavos, I.N., Vergos, G.S., Kotzev, V. & Pashova, L., 2005. Mean sea level and sea surface topography studies in the Black Sea and the Aegean, *in International Association of Geodesy Symposia*, '*Gravity Geoid and Space Missions 2004*', **129**, 254-259, ed. Jekeli, C., Bastos, L., & Fernandes, J., Springer – Verlag Berlin Heidelberg.

Vergos, G.S. & Tziavos, I.N., 2007. Determination of the quasi-stationary sea surface topography from a common adjustment of a geodetic and an oceanographic model, *in 1st International Symposium of the International Gravity Field Service*, *'Gravity Field of the Earth'*, Special Issue **18**, pp. 235-241, eds. Forsberg R., Kiliçoğlu A., General Command of Mapping.

Vergos, G.S., Tziavos, I.N. & Andritsanos, V.D., 2005a. On the determination of marine geoid models by least-squares collocation and spectral methods using heterogeneous data, *in International Association of Geodesy Symposia, 'A Window on the Future of Geodesy'*, **128**, 332-337, ed. Sansò, F., Springer – Verlag Berlin Heidelberg.

Vergos, G.S., Tziavos, I.N. & Andritsanos, V.D., 2005b. Gravity Data Base Generation and Geoid Model Estimation Using Heterogeneous Data, *in International Association of Geodesy Symposia, 'Gravity Geoid and Space Missions 2004'*, **129**, 155-160, eds. Jekeli, C., Bastos, L. & Fernandes, J., Springer – Verlag Berlin Heidelberg.

Wackernagel, H., 2003. *Multivariate Geostatistics*, Springer Verlag, Berlin Heidelberg.

Wenzel, G., 1998. Ultra high degree geopotential models GPM98A, B and C to degree 1800, in *Proc. of Joint Meeting of the Int. Gravity Commission and Int. Geoid Commission*, '*Second Continental Workshop on the Geoid in Europe'*, **98**(4), 71-80, eds. Vermeer, M. and Ádám, J., Finnish Geodetic Institute, Helsinki.

Wenzel, H.G., 1999. Global models of the gravity field of high and ultra-high resolution, *in Lecture Notes of IAG's Geoid School*, ed. F., Milano, Italy, 1999.